



RESEARCH

Open Access



Synaptic proteomics reveal distinct molecular signatures of cognitive change and *C9ORF72* repeat expansion in the human ALS cortex

Zsafia I. Laszlo¹ , Nicole Hindley¹, Anna Sanchez Avila^{1,2}, Rachel A. Kline^{2,3}, Samantha L. Eaton³, Douglas J. Lamont⁴, Colin Smith^{2,5}, Tara L. Spires-Jones^{2,6}, Thomas M. Wishart^{2,3} and Christopher M. Henstridge^{1,2*} 

Abstract

Increasing evidence suggests synaptic dysfunction is a central and possibly triggering factor in Amyotrophic Lateral Sclerosis (ALS). Despite this, we still know very little about the molecular profile of an ALS synapse. To address this gap, we designed a synaptic proteomics experiment to perform an unbiased assessment of the synaptic proteome in the ALS brain. We isolated synaptoneurosomes from fresh-frozen post-mortem human cortex (11 controls and 18 ALS) and stratified the ALS group based on cognitive profile (Edinburgh Cognitive and Behavioural ALS Screen (ECAS score)) and presence of a *C9ORF72* hexanucleotide repeat expansion (*C9ORF72*-RE). This allowed us to assess regional differences and the impact of phenotype and genotype on the synaptic proteome, using Tandem Mass Tagging-based proteomics. We identified over 6000 proteins in our synaptoneurosomes and using robust bioinformatics analysis we validated the strong enrichment of synapses. We found more than 30 ALS-associated proteins in synaptoneurosomes, including TDP-43, FUS, SOD1 and *C9ORF72*. We identified almost 500 proteins with altered expression levels in ALS, with region-specific changes highlighting proteins and pathways with intriguing links to neurophysiology and pathology. Stratifying the ALS cohort by cognitive status revealed almost 150 specific alterations in cognitively impaired ALS synaptic preparations. Stratifying by *C9ORF72*-RE status revealed 330 protein alterations in the *C9ORF72*-RE +ve group, with KEGG pathway analysis highlighting strong enrichment for postsynaptic dysfunction, related to glutamatergic receptor signalling. We have validated some of these changes by western blot and at a single synapse level using array tomography imaging. In summary, we have generated the first unbiased map of the human ALS synaptic proteome, revealing novel insight into this key compartment in ALS pathophysiology and highlighting the influence of cognitive decline and *C9ORF72*-RE on synaptic composition.

Keywords: ALS, Synapse, Proteomics, FTD, *C9ORF72*, Human brain

Introduction

ALS is a devastating neurodegenerative disease, caused by the loss of upper and lower motor neurons. Patients suffer progressive muscle wastage, resulting in paralysis and death, commonly within 3 years of diagnosis. There is no cure, and a greater understanding of ALS pathogenesis is required to change this bleak prognosis.

*Correspondence: chenstridge@dundee.ac.uk

¹ Division of Cellular and Systems Medicine, School of Medicine, University of Dundee, Dundee, Scotland, UK
Full list of author information is available at the end of the article



© The Author(s) 2022. **Open Access** This article is licensed under a Creative Commons Attribution 4.0 International License, which permits use, sharing, adaptation, distribution and reproduction in any medium or format, as long as you give appropriate credit to the original author(s) and the source, provide a link to the Creative Commons licence, and indicate if changes were made. The images or other third party material in this article are included in the article's Creative Commons licence, unless indicated otherwise in a credit line to the material. If material is not included in the article's Creative Commons licence and your intended use is not permitted by statutory regulation or exceeds the permitted use, you will need to obtain permission directly from the copyright holder. To view a copy of this licence, visit <http://creativecommons.org/licenses/by/4.0/>. The Creative Commons Public Domain Dedication waiver (<http://creativecommons.org/publicdomain/zero/1.0/>) applies to the data made available in this article, unless otherwise stated in a credit line to the data.

ALS is strikingly heterogenous, with 90% of cases being sporadic and the rest due to known alterations in a growing number of genes such as *SOD1*, *TARDBP*, *FUS* and *C9ORF72*. Hexanucleotide repeat expansion in *C9ORF72* (*C9ORF72*-RE) accounts for approximately 40% of familial ALS and 5% of sporadic disease, making it the most common genetic cause [1].

Growing genetic, clinical and pathological evidence suggests that ALS and Frontotemporal Dementia (FTD) lie at opposite ends of a disease spectrum. Almost one third of FTD patients have a *C9ORF72*-RE [2]. Approximately 15% of FTD patients also develop ALS and approximately 15% of ALS cases are diagnosed with co-morbid FTD [3]. In the middle of this spectrum are 30–40% of ALS patients that present with more subtle cognitive (ALS cognitive impairment (ALSci)) and/or behavioural (ALS behavioural impairment – ALSbi) change. While these changes do not meet the criteria for FTD diagnosis, they still affect daily life and associate with quicker disease progression [4, 5]. These non-motor symptoms become much more common in the later stages of disease when up to 80% of ALS patients will present with cognitive or behavioural change [6]. Imaging studies highlight the dorsolateral prefrontal cortex (Brodmann Area 9 (BA9)) as a particularly vulnerable area in relation to cognitive decline in ALS, especially with regards to executive dysfunction which is the most common characteristic in ALSci [4, 7–11]. Furthermore, using a combination of cognitive profiling, post-mortem tissue and high-resolution imaging we recently showed that synapse loss in BA9 was associated with lower cognitive performance [12]. This was the first evidence that synapse loss was associated with cognitive change in ALS. Interestingly, recent PET studies in FTD patients revealed synapse loss in frontotemporal cortices that correlated with lower cognitive scores, thus highlighting overlapping synaptic vulnerability between ALSci and FTD [13].

Synapse loss is one of the earliest conserved pathological features across the heterogenous spectrum of ALS, occurring in the periphery at the neuromuscular junction (NMJ) and within the cortex, often before presentation of symptoms [14–16]. Recent transcriptomic and proteomic studies in human ALS brain have also highlighted changes in synaptic genes and proteins [17, 18]. However, protein alterations in small structures such as the synapse can be diluted in whole cell/tissue analyses. Furthermore, deep proteomic profiling of human brain can reveal changes in protein expression that are not highlighted by RNA expression analysis [19, 20]. This highlights the importance of using well-characterised human samples for the development of comprehensive proteomic datasets. There are

no such datasets currently available for the human ALS synapse.

To address this gap, we have isolated synaptically-enriched fractions from ALS and control brain and performed high-resolution proteomic analysis to uncover the changes in the ALS synaptic proteome. We have identified almost 6000 proteins at the human synapse, showcasing the breadth of analysis possible. We provide comprehensive datasets of the synaptic proteome from two cortical brain areas, BA4 (primary motor cortex) and BA9 (dorsolateral prefrontal cortex). Furthermore, we stratified the ALS cohort by cognitive performance and *C9ORF72*-RE status to uncover links between these clinical factors and underlying molecular changes at the synapse. Using a robust bioinformatics approach, we have uncovered specific pathways and proteins altered in the ALS synaptic proteome compared to controls. Importantly, we discovered the presence of a *C9ORF72*-RE has a distinct effect on the synaptic proteome.

This study not only provides valuable datasets for the field, but also strengthens the hypothesis for synaptic dysfunction as an important feature of ALS and highlights proteins and pathways that could be exploited for future therapeutic development.

Materials and methods

Donor characteristics and brain collection

All donors were assessed using the revised El Escorial criteria for diagnosing ALS [21]. Patients were recruited through the Scottish Motor Neurone Disease Register and data collected in the CARE-MND database (Clinical Audit Research and Evaluation). Ethical approval for this register was obtained from Scotland A Research Ethics Committee 10/MRE00/78 and 15/SS/0216. All clinical data were subsequently extracted from the CARE-MND database. Use of patient samples for genetic profiling has been approved by the Chief Scientist Office Scotland; MREC/98/0/56 1989–2010, 10/MRE00/77 2011–2013, 13/ES/0126 2013–2015, 15/ES/0094 2015-present.

The genetic and cognitive status of ALS patients was obtained via the CARE-MND database. Cognition was assessed using the Edinburgh Cognitive and Behavioural ALS Screen (ECAS, [22]) and genetic profile confirmed as previously described [23]. Following completion of the proteomics data it became apparent that one ALS case was incorrectly classified as ALSci and in fact had a normal ECAS score (red symbol in Additional File 2: Fig. S1D). We expect this to have minimal effect as the influence of this one sample will be dampened by the other 8 within the ALSci experimental pool. Whether we physically pool individual samples or generate a mean value from individual samples after western blot, the result is remarkably similar, suggesting the influence of a single

sample is minimal on the overall group result (Additional File 2: Fig. S3).

Use of human tissue for post-mortem studies has been reviewed and approved by the Edinburgh Brain Bank ethics committee and the ACCORD medical research ethics committee, AMREC (ACCORD is the Academic and Clinical Central Office for Research and Development, a joint office of the University of Edinburgh and NHS Lothian, approval number 15-HV-016). The Edinburgh Brain Bank has research ethics committee (REC) approval (21/ES/0087).

Tissue was obtained from the primary motor cortex (BA4) and the dorsolateral prefrontal cortex (BA9) of age/gender matched clinically diagnosed ALS patients (n=11) and control (no neurological condition) individuals (n=18). Summary demographics can be found in Table 1 and individual donor information found in Additional File 3: Table S1.

Preparation of synaptoneurosomes

Total homogenate (TH) and synaptoneurosomes (SNS) preparation was performed as described previously [24, 25], see Additional File 2: Fig. S1A. Briefly, tissue from BA4 and BA9 from each case was homogenised in homogenisation buffer (25 mM HEPES (pH 7.5), 120 mM NaCl, 5 mM KCl, 1 mM MgCl₂, 2 mM CaCl₂, protease inhibitors (Roche #11,836,153,001) and phosphatase inhibitors (Thermo Scientific #A32959)) using glass homogenisers, on ice. The homogenised tissue was then filtered through an 80 µm nylon filter, and a TH aliquot was stored on dry ice. The remainder of the crude homogenate was filtered further through a 5 µm filter (Millipore, SLSV025LS) and centrifuged for 5 min at 1000 g. Pellets were washed in homogenisation buffer and supernatant was disposed. The final pellet was weighed and resuspended in 100 mM Tris-HCL Buffer (pH 7.6) 4% SDS containing 1% protease inhibitor cocktail (Roche

#11,836,153,001) in 1:5 dilution based on pellet weight. Samples were further homogenised by hand and centrifuged at 17,000 g at 4 °C for 20 min, and the supernatant collected. Concentration of the samples were determined using a Micro BCA Protein Assay kit (Thermo Scientific #23,235).

Pooling samples into experimental groups

25 µg of protein from each individual donor was pooled based on the stratification of the subjects (Fig. 1B), to generate 10 experimental pools. This resulted in one representative pooled master sample for each group, along with original samples from individuals, and all samples were stored at -80 °C until further experiments. The 10 pools were as follows: Pool 1—Control BA9 (n=11); Pool 2—ALS BA9 (n=18); Pool 3—Control BA4 (n=11); Pool 4—ALS BA4 (n=18); Pool 5—ALSnoci BA9 (n=9); Pool 6—ALSnoci BA4 (n=9); Pool 7—ALSci BA9 (n=9); Pool 8—ALSci BA4 (n=9); Pool 9—C9ORF72-ve BA9 (n=12); Pool 10—C9ORF72 +ve BA9 (n=6).

Western blot

10 µg of sample was prepared with 4X Laemmli sample buffer (Bio-Rad, #1,610,747), beta-mercaptoethanol and denatured at 95 °C for 5 min. Samples were loaded into 4–20% Tris-Glycine 1.0 mm polyacrylamide precast gels (Thermo Fisher, #WXP42020BOX) along with 5 µl protein ladder (Li-Cor #928–70,000). After electrophoresis, proteins were transferred onto nitrocellulose membrane using precast transfer stacks (Invitrogen, #IB23001) with the iBlot™ 2 Gel Transfer Device (Invitrogen, #IB21001). Membrane was then stained for total protein using REVERT™ 700 Total Protein stain (Li-Cor, REVERT™ 700 Total Protein Stain Kits, #926–11,010) and imaged with the Li-Cor Odyssey system. After imaging, the membrane was destained based on manufacturer's instructions. Membranes were block

Table 1 Summary demographic data of donors. Post-mortem interval, age at death and ECAS score are presented as mean ± S.D. ECAS score was significantly lower in ALSci compared to ALSnoci (*2-tailed *t*-test; *p* = 0.0005). No differences were found between any other group comparisons. Presence of pTDP43 pathology was assessed blind to diagnosis and cases were classed as pTDP43 positive if aggregates were observed anywhere in the paraffin-embedded section

Experimental group	n	Post-mortem interval (hrs)	Age at death (years)	ECAS score (Max. 136)	Gender (% Male)	pTDP43 BA4 (positive cases)	pTDP43 BA9 (positive cases)
Control	11	74 ± 24	66 ± 18		64	0/11	1/11
ALS	18	81 ± 29	64 ± 10		56	15/18	10/18
ALSnoci	9	95 ± 29	66 ± 9	117 ± 5	44	8/9	5/9
ALSci	9	67 ± 24	62 ± 11	99 ± 11*	67	7/9	6/9
ALS c9 -ve	12	88 ± 29	58 ± 9	108 ± 15	58	10/12	6/12
ALS c9 +ve	6	66 ± 27	67 ± 9	108 ± 8	50	5/6	4/6

with 5% milk/TBST or 5% BSA/TBST solution for an hour. Primary antibodies were diluted in the suitable block solution and membranes were incubated overnight at 4 °C. Next day, after extensive washes secondary antibody was diluted in block and incubated for an hour at room temperature, then imaged with the Li-Cor Odyssey system. The details of primary and secondary antibodies are summarized in Additional File 4: Table S2. Total protein stains shown in Additional File 2: Fig. S1D were generated by running 3 µg total protein in 4–20% Tris–Glycine 1.0 mm polyacrylamide precast gels (as above) and performing an Instant Blue total protein stain, per manufacturer instructions (Expedeon). All original blots are found in Additional File 5: Appendix 1.

Tandem mass tagged (TMT) liquid chromatography mass spectrometry (LC–MS/MS)

S-trap processing of samples

100 µg of total protein per experimental group was processed using S-trap mini protocol (Protifi) as recommended by the manufacturer. Samples were applied on the S-trap mini spin column and trapped proteins were washed 5 times with S-TRAP binding buffer. Samples were digested with trypsin (1:50) overnight at 37 °C in 150 µl of TEAB at a final concentration of 100 mM. Peptides from S-Trap mini spin column were eluted by centrifugation at 4000 g for 30 s in 160 µl of 50 mM TEAB, then 160 µl of 2% aqueous formic acid and finally 160 µl of 50% acetonitrile/0.2% formic acid. Resulting tryptic peptides were pooled, dried and quantified using Pierce Quantitative fluorometric Peptide Assay (Thermo Scientific).

10-plex TMT labelling and high pH reverse phase fractionation

Samples were labelled with TMT tags using Pierce High pH Reversed-Phase Peptide Fractionation kit (Thermo Scientific, #84,868) following manufacturer's protocol. Desalted tryptic peptides (37 µg each sample) were dissolved in 100 µl of 100 mM TEAB. The 10 TMT labels were added to different samples after being dissolved in 41 µl of anhydrous acetonitrile. Mixtures were incubated for 1 h at room temperature, 8 µl of 5% hydroxylamine was added per sample to stop the labelling reaction. Samples were mixed, desalted and dried in speed-vac at 30 °C following labelling with TMT. 200 µl of ammonium formate (NH₄HCO₂) (10 mM, pH 9.5) was used to re-dissolve the samples and peptides were fractionated using High pH RP Chromatography. A C18 Column from Waters (XBridge peptide BEH, 130 Å, 3.5 µm 2.1 × 150 mm, Waters, Ireland) with a guard column (XBridge, C18, 3.5 µm, 2.1×10mm, Waters) were used

on an Ultimate 3000 HPLC (Thermo Scientific). Buffer A: 10 mM ammonium formate in milliQ water pH 9.5 and Buffer B: 10 mM ammonium formate, pH 9.5 in 90% acetonitrile were used for fractionation. Fractions were collected at 1 min intervals using a WPS-3000FC autosampler (Thermo Scientific). Column and guard were equilibrated with 2% Buffer B for 20 min at a flow rate of 0.2 ml/min. Separation gradient of column was started 1 min after 190 µl of TMT labelled peptides were injected into the column. Elution of peptides was done with a column gradient of 2% Buffer B to 10% Buffer B in 6 min, and then from 10% Buffer B to 47% Buffer B in 53 min. Column was washed for 15 min in 100% Buffer B and equilibrated at 2% Buffer B for 20 min. Fraction collection resulted in a total of 80 fractions, 200 µl each, as the fraction collection was stopped after 80 min. The total number of fractions concatenated was set to 20 and the content of the fractions was dried and suspended in 50 µl of 1% formic acid prior to analysis with LC–MS.

LC–MS analysis

Mass spectrometry analysis was carried out at the 'FingerPrints' Proteomics Facility, School of Life Sciences, University of Dundee.

Analysis of peptides was performed on a Q-Exactive-HF (Thermo Scientific) mass spectrometer coupled with a Dionex Ultimate 3000 RSLC Nano (Thermo Scientific). LC buffers were the following: buffer A (0.1% formic acid in Milli-Q water (v/v)) and buffer B (80% acetonitrile and 0.1% formic acid in Milli-Q water (v/v)). Aliquots of 5–7.5 µL of each sample were loaded at 10 µL/min onto a trap column (100 µm × 2 cm, PepMap nanoViper C18 column, 5 µm, 100 Å, Thermo Scientific) equilibrated in 0.1% formic acid. The trap column was washed for 5 min at the same flow rate with 0.1% formic acid and then switched in-line with a Thermo Scientific, resolving C18 column (75 µm × 50 cm, PepMap RSLC C18 column, 2 µm, 100 Å). The peptides were eluted from the column at a constant flow rate of 300 nl/min starting from 5% buffer B to 5% buffer B in 8 min, then from 5% buffer B to 35% buffer B in 125 min, and then to 98% buffer B within 2 min. The column was then washed with 98% buffer B for 20 min and re-equilibrated in 5% buffer B for 17 min. The column was kept all the time at a constant temperature of 50 °C.

Q-Exactive HF was operated in data dependent positive ionisation mode. The source voltage was set to 2.4 kV and the capillary temperature was 250 °C. A scan cycle comprised MS1 scan (m/z range from 335 to 1600, with a maximum ion injection time of 50 ms, a resolution of 120,000 and automatic gain control (AGC) value of 3 × 10⁶) followed by 15 sequential dependent MS2 scans (resolution 60,000) of the most intense ions fulfilling predefined

selection criteria (AGC 1×10^5 , maximum ion injection time 200 ms, isolation window of 0.7 m/z, fixed first mass of 100 m/z, NCE/Stepped nce32, spectrum data type: centroid, AGC target of $1e5$, exclusion of unassigned, singly and >6 charged precursors, peptide match preferred, exclude isotopes on, dynamic exclusion time of 45 s). Mass accuracy is checked before the start of samples.

Peptide quantification

The raw mass spectrometric data files obtained for each experiment were collated into a single quantitated data set using MaxQuant (version 1.6.2.10) [26] and searched against the SwissProt subset of the *H. sapiens* Uniprot database (May 2019 release) using the Andromeda search engine software [27]. Enzyme specificity was set to that of trypsin, allowing for cleavage of N-terminal to proline residues and between aspartic acid and proline residues. Other parameters used were: (i) variable modifications, methionine oxidation, deamidation (N,Q) protein N-acetylation, gln—pyro-glu, Phospho(STY); (ii) fixed modifications, cysteine carbamidomethylation; (iii) TMT 10-plex labels; (iv) MS/MS tolerance: FTMS- 10 ppm, ITMS- 0.06 Da; (v) maximum peptide length, 6; (vi) maximum missed cleavages, 2; (vii) maximum of labelled amino acids, 3; and (viii) false discovery rate, 1%. The correction factors for the TMT labelling were also applied.

The mass spectrometry proteomics data have been deposited to the ProteomeXchange Consortium via the PRIDE partner repository (<https://www.ebi.ac.uk/pride/>) with the dataset identifier PXD037393.

Bioinformatic analyses

MaxQuant output files were filtered by number of unique peptides per protein and by missing values. Protein identifications that were assigned with ≥ 2 unique peptides were retained. In addition, those proteins which were not detected in all samples, were excluded. After these robust clean-up steps, there were 5,348 analysis-ready proteins. ALS data was normalised to control and then 1/median normalized to correct for any minor loading variables, generating ratiometric values for each protein for each experimental comparison. We chose a threshold value of 20% as a relevant change in protein expression (≥ 1.2 or ≤ 0.8 ratio change). This value was chosen as post-hoc validation of protein change by modern western blotting technology is sensitive enough to validate these changes [25, 28]. This analysis-ready dataset can be found in Additional File 1: Dataset 1.

Enrichment analysis

All Swiss-Prot ID were inputted into Database for Annotation, Visualisation and Integrated Discovery (DAVID)

software to identify enriched biological themes within the dataset [29, 30]. This database generates a gene-to-gene similarity matrix using a clustering algorithm to classify highly related genes into functionally related groups. As DAVID can only analyse a maximum of 3000 IDs at once, we halved our dataset using a random number generator tool in Excel. Each protein ID was assigned a random number which was then organised by descending order. Group1 and Group2 contained 2674 gene symbols (Additional File 2: Fig. S2D). Clusters were identified using the Functional Annotation Clustering tool. For more information on the statistics and enrichment algorithms, see the original paper and recent update [29, 30].

To identify the enriched Gene Ontology terms (GO) and KEGG pathways we used g:Profiler and ShinyGo v0.75. Swiss-Prot IDs were submitted into the online platforms with the specification of *Homo Sapiens* datasets. Then, enriched terms were downloaded and plotted.

Data visualization

For visualization of enrichment data we used R version 4.1.2, ggplot2 package. For calculating and plotting Venn diagrams, we used the free online software of the Van de Peer Lab: <https://bioinformatics.psb.ugent.be/webtools/Venn/>. For visualizing heatmaps, first, all protein ratiometric values were \log_2 transformed, and the Z-score was counted using the following formula:

$$\frac{\text{ratiometric value} - \text{group mean}}{\text{standard deviation of group}}$$

Heatmaps were plotted using the heatmap.2 module from the gplots package of R software, using hierarchical clustering with Euclidean distance.

Workflow and schematic figures were prepared using BioRender, www.biorender.com.

Array tomography

Tissue was processed for array tomography as previously described [31]. Briefly, fresh post-mortem tissue from BA9 was dissected and fixed in 4% paraformaldehyde in PBS for 2, 3 h. Samples were then dehydrated through ascending ethanol washes (50%, 70%, 90% and 100%, respectively) and incubated in LR White resin (Electron Microscopy Sciences) overnight. Blocks were then placed individually into capsules containing LR White and polymerized overnight at 60 °C. Tissue blocks were cut into serial sections of 70 nm thickness using an ultracut microtome (Leica UC7) with a Histo Jumbo Diamond knife (Diatome, Hatfield, PA). Tissue ribbons were collected on gelatin-coated glass coverslips and permeabilised using a 50 mM glycine solution and blocked for 30 min (0.1% fish skin

gelatin and 0.05% Tween20 in TBS). Afterwards, samples were immunostained with primary antibodies against synaptophysin (1:50, ab8049, Abcam) and synaptopodin (1:50, 21,064-1-AP, Proteintech) overnight. No primary, negative control was included to rule out non-specific binding of the secondary antibodies. The following day, the staining was developed with fluorescently-labelled secondary antibodies (1:50 donkey anti-mouse Alexa fluor 488-ab150105, Abcam; 1:50 donkey anti-rabbit Alexa fluor 594-ab150076, Abcam, respectively) for 30 min and DAPI (1:1000, ab228549, Abcam) for 5 min. Samples were then mounted onto slides with Immumount mounting media. Images were obtained at the same position on each section along the ribbon using a DeltaVision Elite widefield fluorescence microscope (Image solutions) equipped with a CoolSnap digital camera and softWoRx software. High resolution images were obtained with a $63 \times 1.4\text{NA}$ Plan Apochromat objective. At least two image stacks were captured per region for each case. Stacks were aligned using the ImageJ Multistack Reg plugin [32]. All aligned image stacks were then thresholded, segmented and puncta densities measured using a custom MATLAB script. Colocalisation analysis of the segmented images was performed using an in-house Python script. All custom software can be downloaded from GitHub at https://github.com/arraytomographyusers/Array_tomography_analysis_tool and <https://github.com/lewiswilkins/Array-Tomography-Tool>.

Results

To ensure the production of a high-quality proteomics dataset that allows biologically meaningful comparisons to be made, we designed an experiment comprising 29 brain donors (11 healthy controls and 18 ALS cases). Samples were age and gender matched and summary demographic information can be found in Table 1. More detailed individual demographic data can be found in Additional File 3: Table S1.

Our experimental design incorporated disease, brain region, *C9ORF72*-RE status and cognitive profile, as summarised in Fig. 1A, B. To prevent confounding influences of individual samples due to subtle differences in brain handling, sample preparation or protein extraction, we pooled samples into 10 pre-determined experimental groups (Fig. 1B). Pooling produces a representative master sample for each experimental group, generated from multiple individual samples, which can be further analysed for inter-individual variability using other approaches. Pooling provides evidence of protein changes at a population level and minimises the influence of unusually divergent changes driven by individual samples. This is important as data suggests that protein

extraction from human brain is the stage at which most variability is introduced to a proteomics experiment [33]. Essentially, due to the dilution of all individuals into the pooled sample, only robust changes that occur in all or most individuals will emerge within our pool. We have retained all individual samples for validity experiments. Furthermore, it allows the direct comparison of multiple experimental groups at the same time in the same mass-spectrometer, eliminating the natural variability accompanying multiple experimental runs and dramatically reducing equipment runs and costs. We have used this optimised approach in numerous previous publications [25, 28, 34–37].

Synaptoneurosome characterisation

Synaptoneurosome consist of re-sealed presynaptic terminals and postsynaptic spines. We have shown in previous work using transmission electron microscopy that intact synapses with clear pre- and postsynaptic compartments are retained in these preparations [24, 25]. They keep their trans-synaptic connection, membrane proteins and cytosolic proteins, vesicles and organelles. They will also contain tightly bound glial processes (Additional File 2: Fig. S1B). Therefore, synaptoneurosome can provide extensive insight into the synaptic environment but should not be considered as purified synaptic preparations.

The quality of the synaptically-enriched preparations (Additional File 2: Fig. S1C–E) was assessed using well-characterised molecular approaches as described previously [24, 25, 28]. We first confirmed that the nuclear protein lamin was not detected in synaptic preparations and the synaptic protein synaptophysin was enriched (Additional File 2: Fig. S1C). Furthermore, in addition to the 10 experimental pools, all constituent individual samples were run as total protein gels and consistent banding and expression between samples was observed (Additional File 2: Fig. S1D, E).

Bioinformatic characterisation of synaptoneurosome proteome

Following the validation of synaptoneurosome quality, we initiated a bottom-up, discovery, 10-plex TMT LC-MS/MS proteomics workflow (Fig. 1A). All 10 experimental pools were run at the same time, through the same mass-spec, allowing direct comparison and quantification of proteins between groups. In total, 6059 proteins were putatively detected. We filtered these protein IDs based on the stringent identification criteria of 2 or more unique peptides and removed any proteins not detected in one or more groups, yielding 5348 analysis-ready proteins (Additional File 2: Fig. S2A, Additional File 1:

Dataset 1). Therefore, all proteins analysed throughout were identified by ≥ 2 unique peptides and identifiable within all 10 samples, allowing robust comparisons of protein expression to be made between groups. To confirm that our dataset profiled an enriched synaptic proteome, we performed several alignment and enrichment analyses. Firstly, we aligned our filtered dataset with two recent human brain and synapse proteome studies [38, 39]. This revealed $>99\%$ of our dataset matched recently published data (Fig. 1C). We also aligned our data with three synapse proteome databases [40–42], revealing $>90\%$ of our data overlapped (Additional File 2: Fig. S2B). KEGG pathway analysis showed strong enrichment of common neuronal and synaptic pathways (Fig. 1D) and ShinyGO online analyses [43] revealed strong enrichment of synaptic terms in cellular compartment, molecular function, and biological processes (Fig. 1E). Utilising two further enrichment tools (g:Profiler [44] and DAVID functional annotation [29]), we continually reported clear enrichment of synaptic terms (Additional File 2: Fig. S2C, D).

Taken together, this comprehensive analysis revealed strong enrichment of synaptic components in our samples and significant overlap with previously published human proteomic data.

To ensure changes identified by mass-spectrometry truly reflect the protein changes within the samples, we assessed the change in expression of a selection of proteins by western blot. We selected two proteins that were increased in ALS, two that were decreased and two that did not change, to ensure we gathered a range of protein alterations to assess for correlation between the two methodologies. Ratiometric change in protein expression was quantified (by dividing ALS protein intensity by control intensity) and plotted against the proteomics ratiometric data (by dividing ALS protein intensity by control intensity and correcting by $1/\text{median}$), revealing a robust correlation ($R^2 = 0.849$, $p = 0.0032$; Additional File 2: Fig. S3A, B). This suggests the protein changes highlighted by our mass-spectrometry approach, are reflective of the protein changes occurring within our samples as they could be validated using two distinct methodologies. To assess inter-individual variability within our group samples, we randomly selected 6 ALS samples and 6 controls, then blotted for two proteins (Additional File 2: Fig. S3C). While inter-individual variability was high as expected for human samples, the mean population change in expression closely matched the proteomics data generated by pooled samples, showing increases and decreases where expected (Additional File 2: Fig. S3C). This suggests our pooling strategy does generate a population level sample and is representative of our experimental cohort. This also shows that our proteomics approach

can be used to highlight population-level alterations at the synapse, which can then be further analysed post-hoc at an individual sample level.

Synaptic expression of ALS-associated proteins

Confident that we have a synaptically-enriched dataset and a validated proteomics approach, we first looked for ALS-associated proteins within our data. Using four recently published studies [1, 45–47] we collated 58 ALS-associated genes and found the protein product of 37 of them in our dataset (Additional File 2: Fig. S4A). Proteins were described to have altered abundance if their expression changed by more than 20%. This cut off was chosen for a technical reason and is described in the Methods section. Importantly, we see expression changes in some of these proteins including FUS, SOD1, SQSTM1 and MATR3. As observed in previous work [48] we see a remarkably similar 20% decrease in expression of C9ORF72 in the C9ORF72-RE +ve group (Additional File 2: Fig. S4B). Importantly, C9ORF72 forms a molecular complex with SMCR8 and we found SMCR8 levels also drop by a similar 20%. The most significant change is an upregulation of COG3 (part of the Conserved Oligomeric Golgi complex) in ALS BA4 and BA9. COG3 is a recently identified ALS-associated gene [45] and its role is yet to be elucidated in ALS. COG proteins are essential for regulating Golgi processes and influence protein trafficking and glycosylation in neurons, with mutations linked to several neurological disorders [49]. Golgi fragmentation occurs presymptotically in models of ALS and is observed in both familial and sporadic human patients (reviewed in [50]). Interestingly, several members of the COG complex were found to be altered in our dataset, with some increased across all groups (Additional File 2: Fig. S4C, D).

Regional variation in the ALS synaptic proteome

Following this targeted analysis of ALS-associated proteins, we next took a broader look at synaptic protein change between control and ALS samples from both BA4 and BA9. We identified almost 500 proteins in either BA4 or BA9 with altered expression in ALS compared to controls (Additional File 2: Fig. S5A).

When stratified by region, which revealed region-specific changes in protein abundance (Fig. 2A), more than 300 proteins changed in ALS BA4 (236 UP, 82 DOWN) and almost 250 changed in ALS BA9 (168 UP, 82 DOWN) when compared to controls (Additional File 2: Fig. S5A). KEGG pathway analyses using just the up- and downregulated proteins revealed enrichment for inflammatory pathways such as complement and coagulation pathways in both brain areas (Fig. 2B, C). Interestingly, BA4 revealed more diverse changes at the pathway

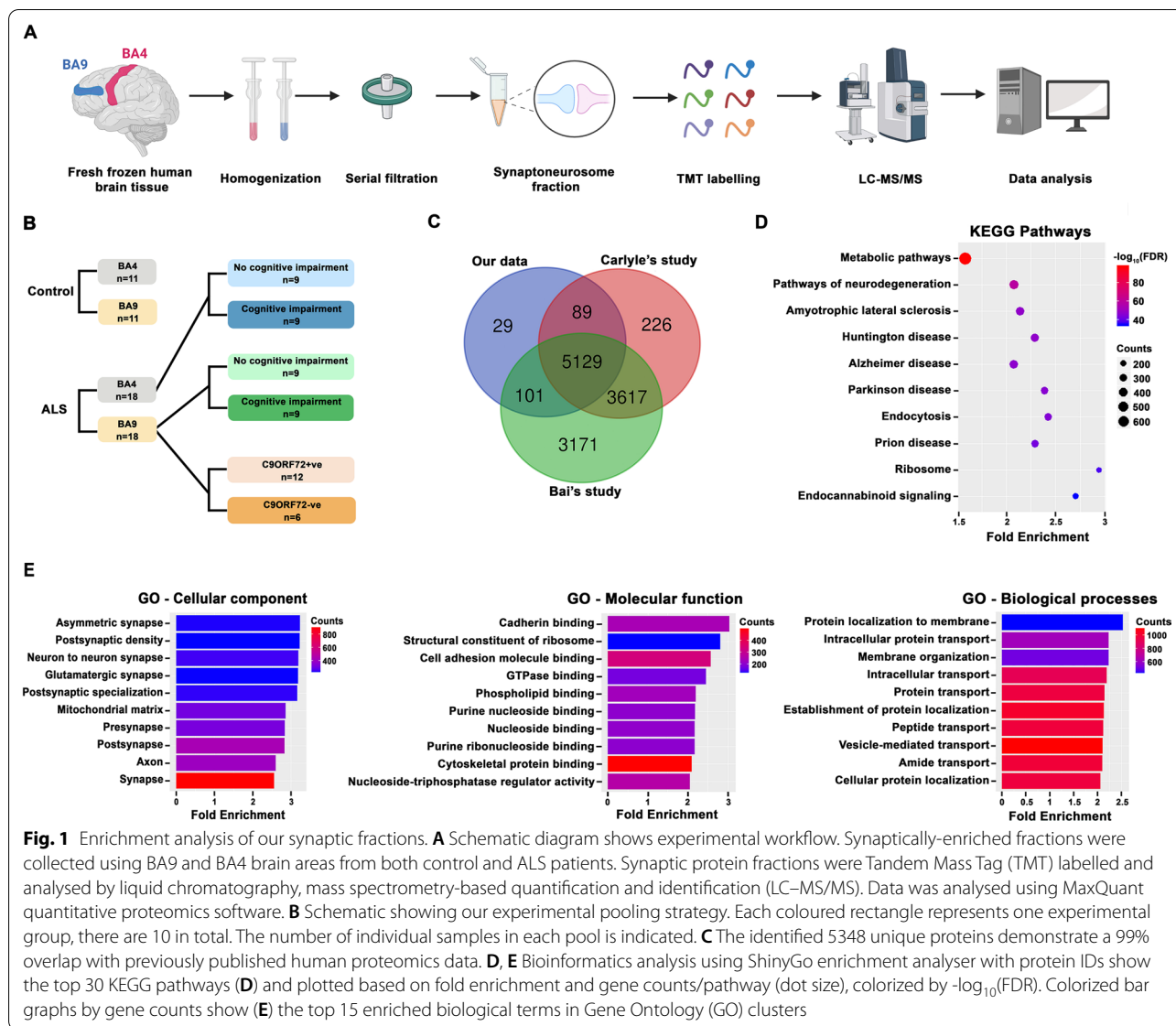


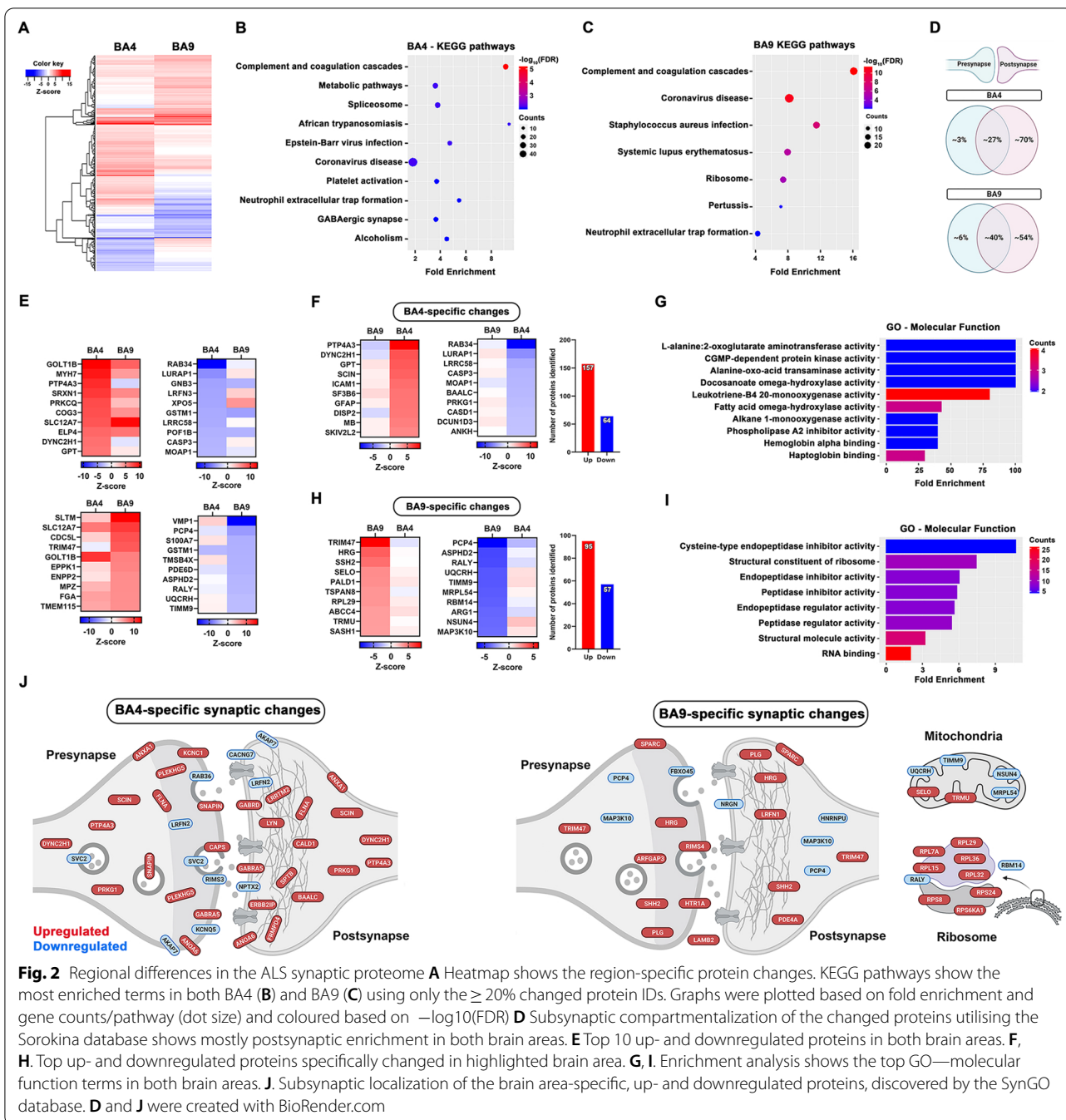
Fig. 1 Enrichment analysis of our synaptic fractions. **A** Schematic diagram shows experimental workflow. Synaptically-enriched fractions were collected using BA9 and BA4 brain areas from both control and ALS patients. Synaptic protein fractions were Tandem Mass Tag (TMT) labelled and analysed by liquid chromatography, mass spectrometry-based quantification and identification (LC-MS/MS). Data was analysed using MaxQuant quantitative proteomics software. **B** Schematic showing our experimental pooling strategy. Each coloured rectangle represents one experimental group, there are 10 in total. The number of individual samples in each pool is indicated. **C** The identified 5348 unique proteins demonstrate a 99% overlap with previously published human proteomics data. **D, E** Bioinformatics analysis using ShinyGo enrichment analyser with protein IDs show the top 30 KEGG pathways (**D**) and plotted based on fold enrichment and gene counts/pathway (dot size), colored by $-\log_{10}(\text{FDR})$. Colored bar graphs by gene counts show (**E**) the top 15 enriched biological terms in Gene Ontology (GO) clusters

level, highlighting the importance of GABAergic signaling and RNA splicing in ALS (Fig. 2B). Following further analysis using the synaptic database by Sorokina and colleagues [40] we discovered that most of the altered proteins were postsynaptic in both brain areas (Fig. 2D). Of the >300 altered proteins in BA4, 221 were specific for that region and KEGG analysis revealed strong enrichment of lipid metabolism pathways (Fig. 2E–G). Next, we submitted the BA4-specific proteins into the experimentally validated SynGO database, which revealed the subsynaptic localization of each protein (Fig. 2J). Despite a small percentage of presynaptic change (Fig. 2D), SynGO highlighted disruption in presynaptic vesicular trafficking (Fig. 2J). Interestingly, postsynaptic glutamate receptor upregulation and cytoskeletal changes dominated.

In BA9, 152 proteins were specifically altered, which were mostly enriched in peptide metabolism and synaptic translation pathways (Fig. 2H, I). As can be seen from Fig. 2J, we also found a remarkable downregulation of key mitochondrial proteins which may reflect mitochondrial stress and energy imbalance at the synapse (Fig. 2J). Several ribosomal proteins were specifically upregulated at the BA9 synapse, possibly highlighting a dysfunction in synaptic RNA processing as an early marker of ALS synaptic stress.

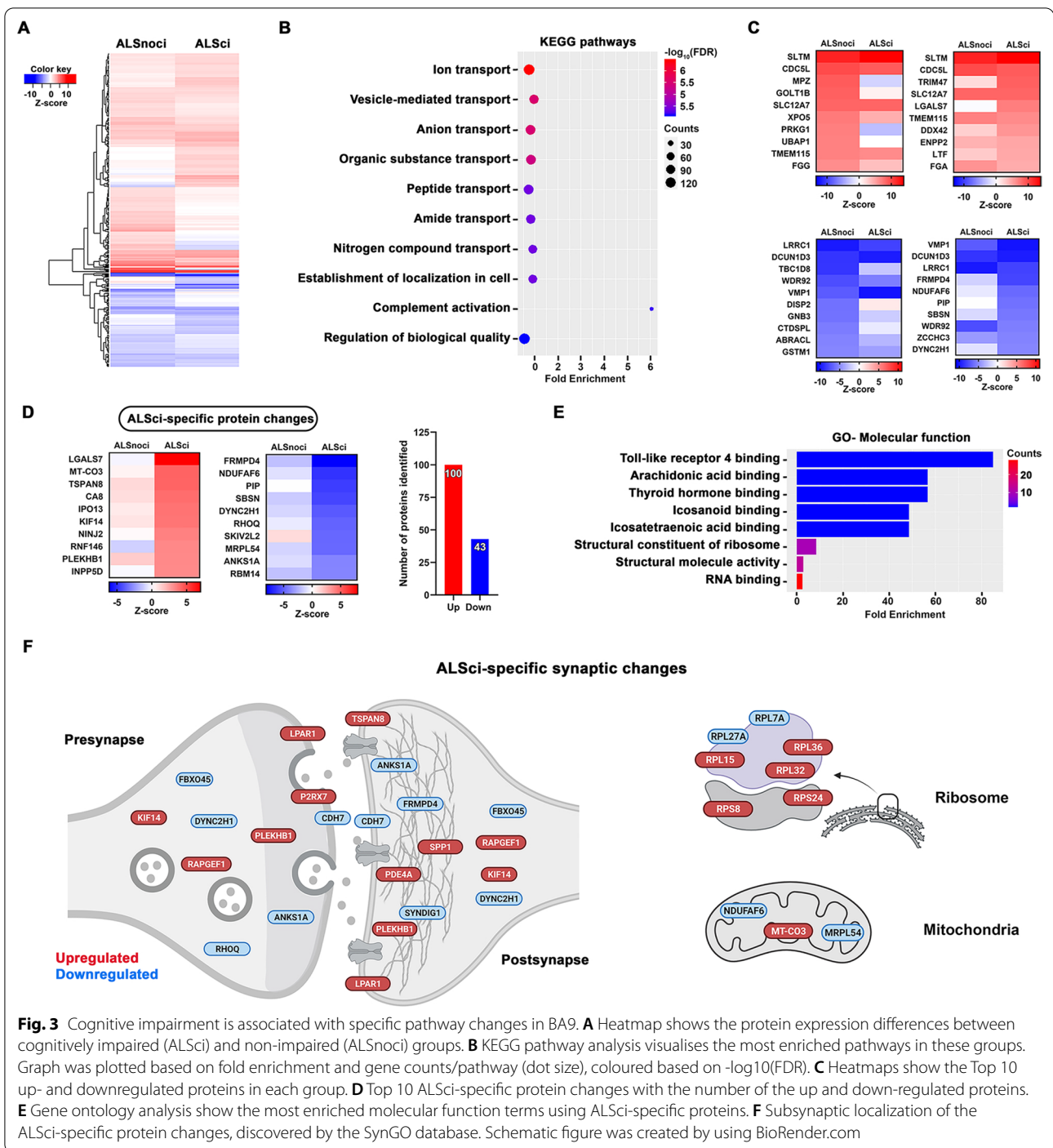
Synaptic protein changes in ALS with cognitive impairment

ALS patients with cognitive impairment (ALSci) have a worse disease prognosis [51] and the underlying



pathophysiology for this is unknown. We previously discovered synaptic loss associated with cognitive decline in BA9 in ALSci [12], however, nothing is known about the molecular changes at the synapse. To address this, we analysed the synaptic proteome in BA4 and BA9 in ALSci samples versus ALS cases with no cognitive impairment (ALS_{noci}) to specifically highlight distinct protein alterations in ALSci synapses. Cognitive function was determined by the extensively validated ECAS test [8].

Patients with a total ECAS scores below 105 were classified as impaired [22]. We discovered altered expression of more than 400 proteins in ALS BA9 compared to control, when samples were stratified by cognitive status (Additional File 2: Fig. S5C, Fig. 3A). Enriched KEGG pathways within the altered proteins include numerous pathways involved in molecular transport and protein localisation and complement pathways (Fig. 3B). More than 260 proteins changed in the ALSci group compared to controls



and 143 of these were specific for the ALSci group, 100 proteins were upregulated and 43 downregulated (Fig. 3C–E). Gene ontology analysis of these 143 proteins revealed enrichment of inflammatory signalling pathways and RNA biology (Fig. 3E). In addition, subsynaptic compartmentalization analysis revealed that important synapse-spanning adhesion (CDH7) and postsynaptic

scaffolding proteins (FRMPD4) are downregulated, meanwhile several ribosomal proteins are upregulated (Fig. 3F).

In BA4 we found a more severe change with over 600 proteins altered across ALSci and ALSnci groups compared to controls (Additional File 2: Figs. 4A, 5B). KEGG pathway analysis of these proteins revealed enrichment

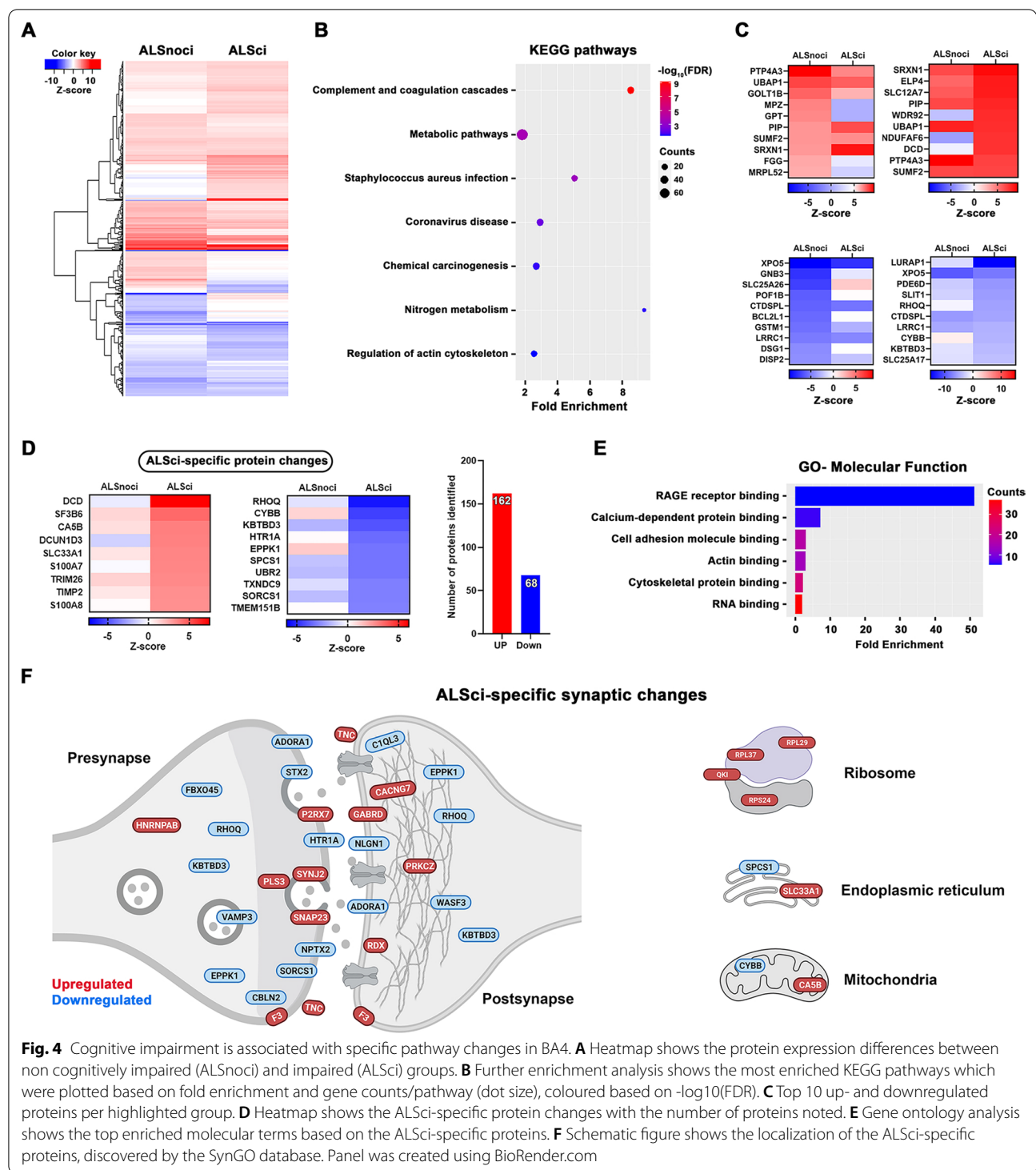


Fig. 4 Cognitive impairment is associated with specific pathway changes in BA4. **A** Heatmap shows the protein expression differences between non cognitively impaired (ALSnoci) and impaired (ALSci) groups. **B** Further enrichment analysis shows the most enriched KEGG pathways which were plotted based on fold enrichment and gene counts/pathway (dot size), coloured based on $-\log_{10}(\text{FDR})$. **C** Top 10 up- and downregulated proteins per highlighted group. **D** Heatmap shows the ALSci-specific protein changes with the number of proteins noted. **E** Gene ontology analysis shows the top enriched molecular terms based on the ALSci-specific proteins. **F** Schematic figure shows the localization of the ALSci-specific proteins, discovered by the SynGO database. Panel was created using BioRender.com

of pathways involved in complement activation, metabolic pathways and the regulation of actin cytoskeleton (Fig. 4B). When stratified by cognitive status we found that ALSci BA4 synapses expressed 271 upregulated and 114 downregulated proteins (Additional File 2: Figs.

S5B and S4C). ALSci-specific synaptic changes in BA4 consisted of 162 upregulated and 68 downregulated proteins (Fig. 4D). Gene ontology of these 230 ALSci-specific proteins in BA4, revealed significant enrichment of RAGE receptor biology, cytoskeleton pathways and RNA

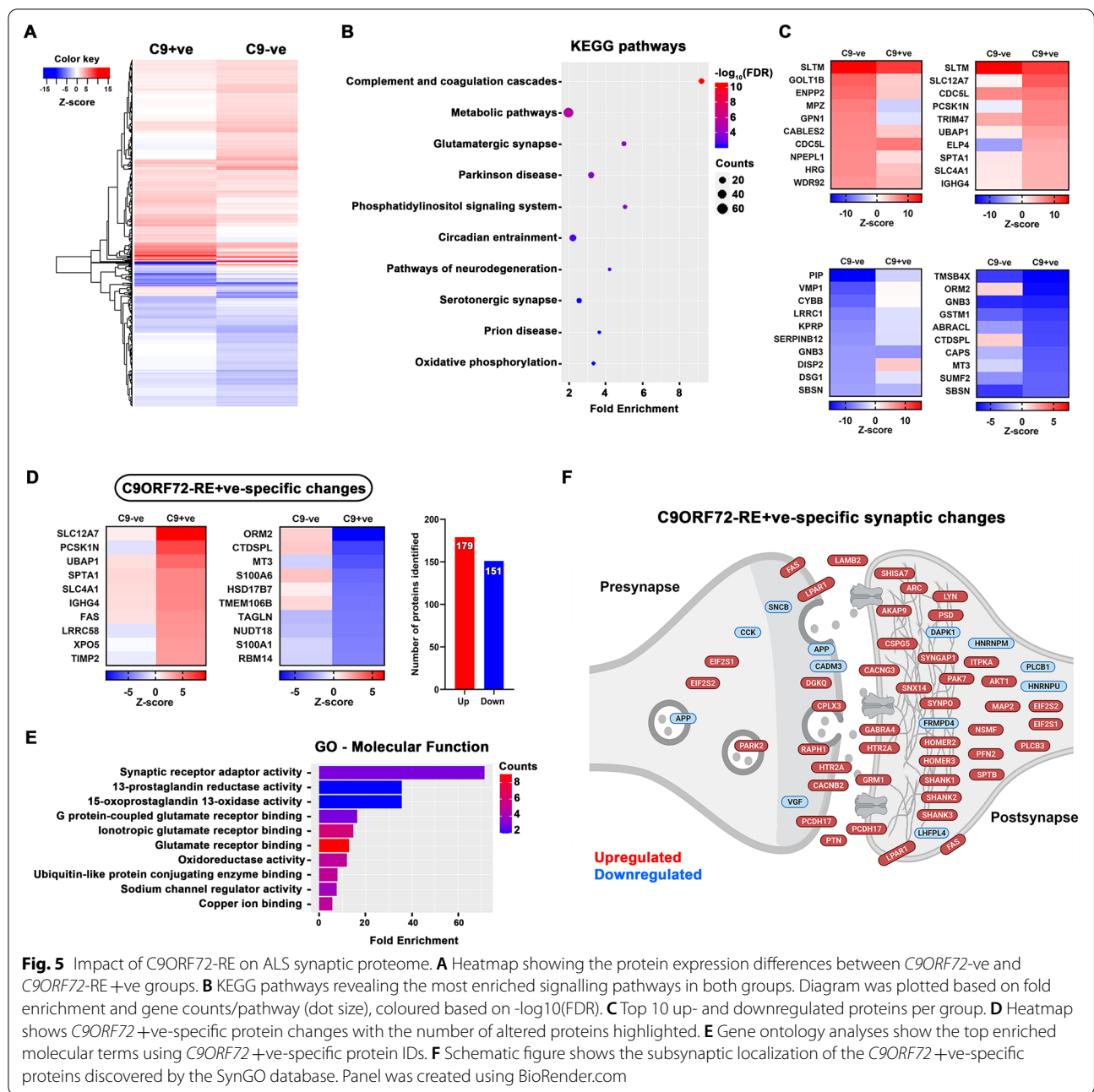


Fig. 5 Impact of C9ORF72-RE on ALS synaptic proteome. **A** Heatmap showing the protein expression differences between C9ORF72-ve and C9ORF72-RE+ve groups. **B** KEGG pathways revealing the most enriched signalling pathways in both groups. Diagram was plotted based on fold enrichment and gene counts/pathway (dot size), coloured based on $-\log_{10}(\text{FDR})$. **C** Top 10 up- and downregulated proteins per group. **D** Heatmap shows C9ORF72+ve-specific protein changes with the number of altered proteins highlighted. **E** Gene ontology analyses show the top enriched molecular terms using C9ORF72+ve-specific protein IDs. **F** Schematic figure shows the subsynaptic localization of the C9ORF72+ve-specific proteins discovered by the SynGO database. Panel was created using BioRender.com

biology (Fig. 4E). Interestingly, subsynaptic analysis identified proteins involved in synaptic vesicle docking and turnover were downregulated, along with several key proteins involved in synaptic adhesion (Fig. 4F).

Impact of C9ORF72-RE on the synaptic proteome

Finally, we assessed the role of C9ORF72-RE on the ALS synaptic proteome by stratifying BA9 samples based on the patient’s C9ORF72-RE status. Analysis of protein changes across both groups revealed almost 600 altered

proteins compared to controls (Additional File 2: Fig. S5A and D). Interestingly, almost twice as many proteins were altered in the C9ORF72-RE+ve group (453) compared to the C9ORF72-RE-ve group (257) when compared to controls (Additional File 2: Fig. S5D). KEGG pathway analysis of all 587 altered proteins across groups, revealed enrichment of complement and metabolism pathways again, but also synaptically-important pathways involving different synapse types (glutamatergic and serotonergic), and neurodegenerative disease pathways such as

Parkinson's and Prion disease (Fig. 5B). Strikingly, 330 of the 453 altered proteins in the *C9ORF72*-RE+ve group, were specifically altered in that group (Fig. 5D). Gene ontology analysis of those 330 proteins revealed significant enrichment of synaptic receptor pathways, with a strong focus on glutamatergic receptor function (Fig. 5E). Interestingly, in confirmation of this, subsynaptic analysis of the *C9ORF72*-RE+ve specific proteins revealed that the majority were found postsynaptically and enriched within the postsynaptic density or the actin cytoskeleton (Fig. 5F). Strikingly, many key synaptic scaffolding proteins such as Shanks and Homers were upregulated. In addition, we found that several presynaptic vesicular proteins were altered, which may result in the malfunction of neurotransmitter release. The dramatic postsynaptic changes may be an attempt to compensate for presynaptic dysfunction (Fig. 5F).

To confirm if the dramatic postsynaptic change is reflective of changes in the intact brain, we analysed expression and localisation of two proteins at the single synapse level using array tomography. We selected the unchanged presynaptic protein synaptophysin and the upregulated postsynaptic scaffolding protein synaptopodin and compared their expression in 3 randomly selected control, *C9ORF72*-ve and *C9ORF72*+ve cases. Both antibodies produced beautiful synapse-like puncta throughout the BA9 cortical neuropil (Additional File 2: Fig. S6A). Synaptopodin puncta were typically found directly opposed to the presynaptic protein synaptophysin (Additional File 2: Fig. S6B), as expected for a postsynaptic protein [52]. There was no change in synaptophysin density, in agreement with the proteomics data. However, analysis of synaptopodin density revealed an approximate 28% change in *C9ORF72*+ve cases compared to *C9ORF72*-ve cases, which is remarkably similar to the 27% increase observed using proteomics (Additional File 2: Fig. S6C).

Discussion

In this study we have profiled for the first time, the synaptic proteome in human ALS, revealing regional, genotypic and phenotypic differences. Using an unbiased high-resolution proteomic approach, we have identified hundreds of altered proteins in two key brain areas associated with ALS clinical presentation and assessed the influence of the most common genetic cause of ALS/FTD, *C9ORF72*-RE. We have performed extensive molecular and bioinformatic validation of our proteomics dataset and confirmed some changes at a single synapse resolution in intact human post-mortem material.

We identified more than 6000 proteins in the human cortical synaptoneurosome fraction and highlight significant overlap of our dataset with several published

human proteomic studies and online proteomic datasets. This preparation consists of resealed presynaptic terminals and postsynaptic spines, along with bound glial processes. This provides critical proteomic insight on the full synaptic composition, rather than isolated presynapses or postsynaptic densities, as is common with other synaptic studies. Stringent filtering of our dataset resulted in 5348 analysis-ready proteins which we robustly show are enriched in synapses. However, it is important to consider this to be an enriched and not purified synaptic fraction and to realise the limitations of "bottom-up" proteomics, resulting in the loss of information on post-translational modification and some protein isoforms.

Assessing the changes across the brain in all ALS cases and controls, we identified altered expression of 470 proteins. KEGG pathway analysis highlighted inflammatory processes, synapse subtypes and intriguing ALS-associated pathways such as the spliceosome (Fig. 2B, C). Neuroinflammation is a common feature of nearly all neurodegenerative diseases and has been reviewed previously in ALS [53]. Inflammatory proteins at the synapse could appear due to non-autonomous changes in the synaptic milieu or increased synaptic expression of proteins typically considered to be non-neuronal. For example, the complement system is a key feature of the innate immune system [54] but certain components are expressed at synapses, tagging them for removal by microglia [55]. This has recently been shown to be a driver of Alzheimer's disease pathogenesis [56] and our data revealing increased expression of several complement proteins at the ALS synapse, may suggest a similar process renders ALS synapses vulnerable to aberrant removal. Glutamate excitotoxicity is important in ALS pathogenesis and is driven by excessive activity of excitatory neurons. This could be due to intrinsic changes in neuronal firing properties or reduced inhibitory control by GABAergic cells. It is therefore interesting to note that, "GABAergic synapse" was enriched in our BA4 KEGG analyses and may highlight inhibitory networks as a sight of vulnerability in ALS (Fig. 2B). This has been suggested in ALS models and post-mortem human material [57–59]. Alternative splicing of many RNA targets is altered in ALS [60] and key splicing factors and RNA binding proteins are known to function in or near synapses [61, 62]. We find the spliceosome enriched within BA4 ALS synapses, and it would be important to unravel what effect this may have on the splicing and subsequent composition of synaptic proteins, especially given recent data linking TDP-43 mislocalisation to aberrant splicing and decreased expression of the synaptic protein Munc13-1 (UNC13A) [63, 64].

Looking at the individual protein level, there were many changes consistent across cortical regions. For

example, SLC12A7 is a $K^+ - Cl^-$ co-transporter (also called KCC4) that maintains intracellular Cl^- concentration (critical for balancing neuronal ionic gradients) and plays an important role in regulating cell size by mediating ion transport in response to cell swelling [65]. KCC4 was within the top 10 upregulated proteins in both BA4 and BA9 (Fig. 2E), possibly as a shared compensatory mechanism to correct fluctuating neuronal ionic gradients or as a result of cell soma and axonal swelling, a known pathological feature of ALS [66, 67]. Furthermore, GSTM1 (glutathione S-transferase, mu subtype 1) was decreased in both BA4 and BA9 synaptoneuroosomes (Fig. 2E). GSTM1 is exclusively expressed in astrocytes in mouse brain and is involved in proinflammatory activation of microglia during neuroinflammation [68]. We also observed increased expression of GFAP in BA4 (Fig. 2F), highlighting complex bidirectional changes in astrocytic proteins around ALS synapses. This has gained added significance following a recent study highlighting GFAP-containing tripartite synapses as the most vulnerable subtype in ALS spinal cord [69].

Region-specific alterations

Looking at region-specific changes, we found a significant increased expression of PTP4A3 (also known as PRL-3) in BA4 (Fig. 2F). PRL-3 is a phosphatase highly expressed in several cancers, increasing cell proliferation and survival [70]. Very little is known about its physiological role in the brain, however a recent paper [71] highlighted a critical role for the *Drosophila* orthologue (prl-1) in axonal arborisation and synaptogenesis. This may suggest that PRL-3 is significantly upregulated in our data as a compensatory response to retain axonal complexity and synaptic connectivity within a degenerating motor cortex.

Rab34 was significantly and specifically downregulated in BA4 synapses (Fig. 2F). Rab34 is a member of the Ras-related proteins in brain (Rab) family, which is involved in intracellular vesicle trafficking and phagosome/lysosome dynamics. Rab34 plays a role in the positioning of lysosomes [72] but is also known to interact with the synaptic vesicle priming protein Munc13-2 [73, 74]. Munc13-2 is important for vesicle priming and is often co-expressed in the same synapses as Munc13-1 [75]. Mutations in the Munc13-1 gene (UNC13A) are causative for ALS and two recent papers highlight TDP-43-dependent alterations in UNC13A and decreased protein product [63, 64]. Therefore, decreased expression of Rab34 at BA4 synapses may render these vulnerable due to inefficient vesicle priming and disrupted synaptic transmission. We discovered Munc13-1 at the synapse but did not see a change in expression level, likely due to the mixed population of

synapses collected from neurons with/without TDP-43 mislocalisation.

In the frontal cortex, TRIM47 was specifically upregulated more than twofold compared to control synapses (Fig. 2H). TRIM47 is an E3 ubiquitin-protein ligase that mediates the degradation of CYLD lysine 63 deubiquitinase (CYLD) [76], which has very recently been highlighted as a rare causative gene for FTD [77, 78] and possibly ALS [79]. Interestingly, CYLD is known to interact with proteins already implicated in ALS/FTD, such as TBK1, OPTN and SQSTM1 [77]. Few cases have been described and there is debate around what effect the disease-associated mutations have on CYLD activity [79, 80], however it is interesting to note that the most upregulated protein in the ALS frontal cortex is known to regulate levels of a protein directly implicated in FTD. Supporting the link between TRIM47 and cognitive change, TRIM47 was increased more than twofold in the ALSci samples. TRIM47 has also been recently shown to accelerate brain injury after cerebral ischaemia/reperfusion, with TRIM47 knockdown being both neuroprotective and anti-inflammatory [81]. Therefore, increased TRIM47 expression may indicate inflammatory processes at play within the synaptic milieu.

PCP4 (also known as PEP-19) is a calcium/calmodulin binding protein which regulates calmodulin function by modulating its interaction with calcium [82]. PEP-19 is expressed in the cortex of post-mortem human brain and its levels are significantly decreased in Alzheimer's, Huntington's and Parkinson's disease [83]. PEP-19 knockout in mice produces significant alterations in synaptic plasticity and behaviour, likely due to its loss of control over calmodulin activity, a key process in synaptic plasticity [84]. Here, we discovered a specific decrease of PEP-19 in synapses of the ALS frontal cortex (Fig. 2H), introducing PEP-19 as a potential new player in ALS synaptic dysfunction.

Synaptic alterations in ALSci

ALSci patients have a worse prognosis and present with cognitive and behavioural changes, reminiscent of FTD [51]. We recently discovered that ALSci cases have synapse loss in the frontal cortex [12] and in this study we stratified our samples by cognitive status to try and uncover the molecular changes that may influence synaptic integrity. We identified 143 proteins specifically altered in the ALSci BA9 samples and gene ontology analysis revealed enrichment of toll-like receptor 4 (TLR4) pathways (Fig. 3E), critical components of the innate immune system. Recent work has shown TLR4-dependent synapse loss after traumatic brain injury, which could be reduced by TLR4 blockade [85]. Furthermore, TLR4 knockout in hSOD1G93A mice leads to

improved grip strength and extended survival [86]. TLR4 induction also leads to increased synapse loss around spinal motor neurons in peripheral nerve crush models [87]. Together, this suggests our observation of TLR4 pathway enrichment is likely to be detrimental to synaptic function and structure.

RNF146 (also known as Iduna) is an E3 ubiquitin ligase that uses poly (ADP ribose) (PAR) to recognise its substrates [88], tagging them for degradation, and here is specifically upregulated in ALSci synapses (Fig. 3D). PAR polymerases (PARPs) add PAR motifs to target proteins, with PARP1 being the most prolific [89]. PARP1 initiates a form of cell death known as parthanatos [90] and recent studies describe increased PARP1 activity in ALS spinal motor neurons and the beneficial effects of a small molecule PARP inhibitor [91, 92]. Interestingly, Iduna is an NMDA-receptor induced survival molecule that interferes with parthanatos [93]. Iduna is normally expressed at very low levels in neurons, but following NMDA receptor activation or neuronal stress, Iduna levels significantly increase and have a neuroprotective effect [93]. Therefore, increased RNF146 expression may represent a pro-survival signal retained within stressed synapses, or disease associated RNF146 increase may drive ubiquitination and subsequent degradation of important synaptic proteins.

FRMPD4 was the most significantly decreased protein in ALSci BA9 (Fig. 3D). FRMPD4 is a PSD-95 binding protein that regulates dendritic spine morphogenesis and interacts with Homer and mGluR1/5 to regulate downstream signalling [94, 95]. Furthermore, mutations in FRMPD4, resulting in significant protein loss, have been linked to a severe form of intellectual disability [96]. Interestingly, a recent transcriptomic study in the frontal cortex of sporadic FTD cases, identified a decrease in FRMPD4 expression [97]. Together, this advances the cognitive and pathological overlap between ALSci and FTD to the synaptic level, and highlights FRMPD4 as a key synaptic protein affected in both diseases.

Given the worse prognosis of ALSci patients, we hypothesised these patients may have a more aggressive form of disease, resulting in a distinct molecular change in their BA4 synapses. We discovered 230 specifically altered proteins in the ALSci BA4 samples, and gene ontology analysis highlighted strong enrichment of RAGE receptor pathways (Fig. 4E). In fact, numerous RAGE receptor ligands were upregulated in BA4 synapses, including several S100 calcium-binding proteins. RAGE receptor activation leads to the strong induction of pro-inflammatory signals and increased expression has been shown at presymptomatic stages of SOD1 and TDP43 mouse models of ALS [98]. Furthermore, RAGE knockout in hSOD1^{G93A} mice leads to reduced

inflammation and extended lifespan [98]. In a recent human dataset a negative association between high RAGE expression and earlier age at death was observed [99], supporting our idea that ALSci patients have a more severe form of disease, and this may be driven by RAGE-dependent mechanisms.

Interestingly, we observed a significant decrease in synaptic expression of HTR1A, (the 5HT1A serotonin receptor) in BA4 of ALSci samples (Fig. 4D). Previous human PET imaging revealed a decrease in 5HT1A receptor binding in the cortex (motor and extra-motor regions) of ALS patients versus controls [100]. ALS patients were not tested for cognitive impairment, so data cannot be stratified to assess any association between ALSci and 5HT1A reduction. Here we identified a loss of 5HT1A receptor in the motor cortex of ALSci patients, but surprisingly found an increased expression in BA9. This may reflect synaptic changes at different disease stages, as the disease spreads forward from motor to non-motor regions.

The impact of C9ORF72-RE on synaptic proteome

The physiological role of the C9ORF72 protein is not fully understood, but it is believed to regulate vesicle trafficking and autophagy by interacting with Rab proteins [101]. Furthermore, recent studies have revealed C9ORF72 to be presynaptic and to interact with Rabs involved in synaptic vesicle trafficking [48, 102, 103]. This has been reinforced in iPSC-derived neurons from C9ORF72-RE patients, showing presynaptic dysfunction and altered neuronal network activity [104, 105]. Given the growing literature on the synaptic localisation and function of C9ORF72, we stratified our BA9 samples by the patient's C9ORF72-RE status. There were 587 altered proteins, regardless of C9ORF72-RE status and KEGG pathway analysis highlighted enrichment of inflammatory pathways, but also synaptic subtypes (glutamatergic and serotonergic) and several disease-associated pathways such as Parkinson's disease and prion disease (Fig. 5B). 453 proteins were altered in the C9ORF72-RE +ve group, of which a remarkable 330 were specifically altered (Fig. 5D). Interestingly, gene ontology analysis highlighted enrichment of synaptic receptor pathways, specifically post-synaptic glutamatergic pathways (Fig. 5E), reinforcing the influence of glutamate-induced hyperexcitability in C9ORF72-associated ALS [106]. Metabotropic glutamate receptor 1 and important scaffolding proteins (SynGAP1, Shanks and Homers) were all upregulated (Fig. 5F). This dramatic postsynaptic reorganisation may be a response to altered presynaptic function. We discovered several proteins involved in vesicular trafficking

and homeostasis to be altered at the presynapse. It fits that decreased expression of C9ORF72 protein as a result of C9ORF72-RE, may impact presynaptic function which results in a compensatory reorganisation of the postsynapse to try and maintain synaptic balance. We have also shown for the first time at the single-synapse level in intact human tissue, that postsynaptic scaffolding proteins such as synaptopodin are upregulated in C9ORF72-RE +ve cases (Additional File 2: Fig. S6). Furthermore, increased expression of synaptotagmin-13 is of note, due to recent work suggesting this presynaptic vesicular protein is preferentially expressed in resilient neurons in ALS and Syt13 gene therapy increased survival of SOD1^{G93A} ALS mouse models [107]. These results highlight the complexity of compensatory pre and postsynaptic protein alterations to try and maintain synaptic integrity.

Increasing more than twofold was PCSK1N, also known as pro-SAAS (Fig. 5D). This small secretory chaperone is expressed throughout the brain [108] and has been linked to several neurodegenerative diseases, including FTD [109–112]. Pro-SAAS can prevent fibrillation of disease associated proteins such as amyloid [113] and α -synuclein [114], suggesting it may serve important neuroprotective roles. Importantly, several ALS-associated proteins undergo fibrillation and subsequent aggregation, such as TDP-43 [115] and the dipeptide repeats (DPRs) generated from C9ORF72-RE [116]. Therefore, this may suggest that pro-SAAS upregulation at the C9ORF72-RE +ve synapses is an attempt to combat fibrillation and aggregation of disease-associated proteins.

Strikingly, TMEM106B was specifically decreased in the C9ORF72-RE +ve samples (Fig. 5D). TMEM106B is involved in lysosomal homeostasis and overexpression leads to abnormalities in lysosomal acidification, size and number [117]. *TMEM106B* is a genetic risk factor for FTLTDP, especially in patients with granulin mutations [118], yet intriguingly the same alleles appear protective for C9ORF72-RE carriers, resulting in later age of onset and death [119]. Furthermore, TMEM106B knockout in a granulin model of ALS, leads to reversal of lysosomal alterations and prevention of neurodegeneration [120]. Therefore, specific reduction of TMEM106B in C9ORF72-RE +ve samples may be a compensatory attempt to regulate lysosomal function, or a concomitant loss of lysosomal proteins due to C9ORF72-RE-dependent lysosomal dysfunction. Alternatively, lower synaptic expression of TMEM106B may be due to mislocalisation and aggregation in other neuronal compartments, as recently shown in FTLTDP [121]. Finally, TMEM106B knockdown leads to altered lysosomal trafficking and reduced dendritic

arborisation [122], so a loss of TMEM106B at the synapse may drive vulnerability.

Conclusions

In summary, we have mapped the first unbiased proteome of the human ALS synapse, uncovering novel players in synaptic dysfunction and highlighting ALS-associated proteins in this vulnerable subcellular compartment. It is important to note the complexity of a synaptoneurosomal fraction and the limitations of a bottom-up proteomics workflow when interpreting the data. However, this work has strengthened many previous findings implicating ALS-associated proteins at the synapse and revealed hundreds of new proteins and pathways for future exploitation. Importantly, future work in model systems will uncover the mechanisms leading to these protein changes, adding critical insight into ALS pathogenesis, and highlighting novel avenues of understanding and therapeutic development.

Abbreviations

ALS: Amyotrophic lateral sclerosis; ALSnoc: Amyotrophic lateral sclerosis with no cognitive impairment; ALSci: Amyotrophic lateral sclerosis with cognitive impairment; BA4: Brodmann area 4—Primary motor cortex; BA9: Brodmann area 9—Dorsolateral prefrontal cortex; C9ORF72-RE: C9ORF72 Hexanucleotide repeat expansion; DAVID: Database for annotation, visualisation and integrated discovery; ECAS: Edinburgh cognitive and behavioural ALS screen; FTD: Frontotemporal dementia; GO: Gene ontology; KEGG: Kyoto encyclopedia of genes and genomes; TMT: Tandem mass tagging.

Supplementary Information

The online version contains supplementary material available at <https://doi.org/10.1186/s40478-022-01455-z>.

Additional file 1. Complete analysis ready dataset containing all protein identifications associated with the manuscript.

Additional file 2. All Supplementary Figures and legends.

Additional file 3. Supplementary Table 1, extended patient cohort information.

Additional file 4. Supplementary Table 2, primary antibody information.

Additional file 5. Appendix 1, example images from whole western blots used in this manuscript

Acknowledgements

We gratefully acknowledge the generous donors who have made this work possible. We wish to acknowledge the CARE-MND Register, hosted by the Euan Macdonald Centre (EMC) for MND Research and funded by MND Scotland. We are extremely thankful for the hard work of the Scottish MND Clinical Specialist Team for obtaining consent for tissue donation, led by Judith Newton. We thank Dominic Kurian from the Roslin Institute Proteomic and Metabolomic Facility for advice.

Author contributions

ZIL performed experiments, data analysis and prepared the manuscript. NH and ASA performed experiments and edited the manuscript. RAK and SLE performed experiments and edited the manuscript. DJL provided the proteomics service. CS provided human tissue. TLS-J and TMW helped design the study, provided resources, mentorship and edited the manuscript. CMH designed

the study, performed experiments, analysed data and wrote the manuscript. All authors read and approved the final manuscript.

Funding

CMH acknowledges funding support from MND Scotland, TENOVUS Scotland and Alzheimer's Research UK (ARUK-EG2019B-003). This work was funded by a Lady Edith Wolfson Junior Non-Clinical Fellowship to Z.I.L from the MND Association (Laszlo/Oct21/977-799). ASA is funded by a Euan Macdonald Centre for Motor Neuron Disease Research PhD studentship. TSJ receives funding from the European Research Council (ERC) under the European Union's Horizon 2020 research and innovation programme (grant agreement no. 681181) and the UK Dementia Research Institute which receives its funding from DRI Ltd, funded by the UK Medical Research Council, Alzheimer's Society, and Alzheimer's Research UK. RAK was funded by the Euan Macdonald Centre for Motor Neuron Disease Research PhD studentship, and the University of Edinburgh's Principal's Career Development and Global Research scholarships. TMW and SLE are supported by funding from the Biotechnology and Biological Sciences Research Council (BBSRC) Institute Strategic Grant No. (BBS/E/D/10002071).

Availability of data and materials

Analysis-ready datasets are included as Supplementary data and original RAW mass spectrometry files are available via ProteomeXchange with identifier PXD037393.

Declarations

Ethics approval and consent to participate

Patients were recruited through the Scottish Motor Neurone Disease Register and data collected in the CARE-MND database (Clinical Audit Research and Evaluation). Ethical approval for this register was obtained from Scotland A Research Ethics Committee 10/MRE00/78 and 15/SS/0216. All clinical data were subsequently extracted from the CARE-MND database. Use of patient samples for genetic profiling has been approved by the Chief Scientist Office Scotland; MREC/98/0/56 1989–2010, 10/MRE00/77 2011–2013, 13/ES/0126 2013–2015, 15/ES/0094 2015–present. Use of human tissue for post-mortem studies has been reviewed and approved by the Edinburgh Brain Bank ethics committee and the ACCORD medical research ethics committee, AMREC (ACCORD is the Academic and Clinical Central Office for Research and Development, a joint office of the University of Edinburgh and NHS Lothian, approval number 15-HV-016). The Edinburgh Brain Bank has research ethics committee (REC) approval (21/ES/0087).

Consent for publication

All authors have read the manuscript and agreed with its submission.

Competing interests

The authors declare that they have no Competing interests.

Author details

¹Division of Cellular and Systems Medicine, School of Medicine, University of Dundee, Dundee, Scotland, UK. ²The Euan Macdonald Centre, Edinburgh, UK. ³The Roslin Institute, Royal (Dick) School of Veterinary Studies, College of Medicine and Veterinary Medicine, University of Edinburgh, Edinburgh EH25 9RG, Scotland, UK. ⁴FingerPrints Proteomics Facility, Discovery Centre, School of Life Sciences, University of Dundee, Dundee, Scotland, UK. ⁵Academic Neuropathology, Centre for Clinical Brain Sciences, University of Edinburgh, Edinburgh, Scotland, UK. ⁶Centre for Discovery Brain Sciences and UK Dementia Research Institute at the University of Edinburgh, Edinburgh, UK.

Received: 29 September 2022 Accepted: 30 September 2022

Published online: 29 October 2022

References

- Mejzini R, Flynn LL, Pitout IL, Fletcher S, Wilton SD, Akkari PA (2019) ALS genetics, mechanisms, and therapeutics: where are we now? *Front Neurosci* 13:1310
- Abramzon YA, Fratta P, Traynor BJ, Chia R (2020) The overlapping genetics of amyotrophic lateral sclerosis and frontotemporal dementia. *Front Neurosci* 14:42
- Ling SC, Polymenidou M, Cleveland DW (2013) Converging mechanisms in ALS and FTD: disrupted RNA and protein homeostasis. *Neuron* 79(3):416–438
- Goldstein LH, Abrahams S (2013) Changes in cognition and behaviour in amyotrophic lateral sclerosis: nature of impairment and implications for assessment. *Lancet Neurol* 12(4):368–380
- Strong MJ, Abrahams S, Goldstein LH, Woolley S, McLaughlin P, Snowden J et al (2017) Amyotrophic lateral sclerosis - frontotemporal spectrum disorder (ALS-FTSD): revised diagnostic criteria. *Amyotroph Lateral Scler Frontotemporal Degener*. <https://doi.org/10.1080/21678421.2016.1267768>
- Crockford C, Newton J, Lonergan K, Chiwera T, Booth T, Chandran S et al (2018) ALS-specific cognitive and behavior changes associated with advancing disease stage in ALS. *Neurology* 91(15):e1370–e1380
- Abrahams S, Goldstein LH, Kew JJ, Brooks DJ, Lloyd CM, Frith CD et al (1996) Frontal lobe dysfunction in amyotrophic lateral sclerosis. A PET study *Brain* 119(Pt 6):2105–2120
- Abrahams S, Newton J, Niven E, Foley J, Bak TH (2014) Screening for cognition and behaviour changes in ALS. *Amyotroph Lateral Scler Frontotemporal Degener* 15(1–2):9–14
- Canosa A, Pagani M, Cistaro A, Montuschi A, Iazzolino B, Fania P et al (2016) 18F-FDG-PET correlates of cognitive impairment in ALS. *Neurology* 86(1):44–49
- Menke RAL, Agosta F, Grosskreutz J, Filippi M, Turner MR (2017) Neuroimaging endpoints in amyotrophic lateral sclerosis. *Neurotherapeutics* 14:11–23
- Turner MR, Agosta F, Bede P, Govind V, Lule D, Verstraete E (2012) Neuroimaging in amyotrophic lateral sclerosis. *Biomark Med* 6(3):319–337
- Henstridge CM, Sideris DJ, Carroll E, Rotariu S, Salomonsson S, Tzioras M et al (2018) Synapse loss in the prefrontal cortex is associated with cognitive decline in amyotrophic lateral sclerosis. *Acta Neuropathol* 135(2):213–226
- Malpetti M, Jones PS, Cope TE, Holland N, Naessens M, Rouse MA, et al. (2022) Synaptic loss in behavioural variant frontotemporal dementia revealed by [11C]UCB-J PET. *medRxiv*. 2022:2022.01.30.22270123
- Fogarty MJ (2018) Driven to decay: excitability and synaptic abnormalities in amyotrophic lateral sclerosis. *Brain Res Bull* 140:318–333
- Fogarty MJ (2019) Amyotrophic lateral sclerosis as a synaptopathy. *Neural Regen Res* 14(2):189–192
- Henstridge CM, Pickett E, Spiers-Jones TL (2016) Synaptic pathology: a shared mechanism in neurological disease. *Ageing Res Rev* 28:72–84
- Umoh ME, Dammer EB, Dai J, Duong DM, Lah JJ, Levey AI et al (2018) A proteomic network approach across the ALS-FTD disease spectrum resolves clinical phenotypes and genetic vulnerability in human brain. *EMBO Mol Med* 10(1):48–62
- Dols-Icardo O, Montal V, Sirisi S, López-Pernas G, Cervera-Carles L, Querol-Vilaseca M et al (2020) Motor cortex transcriptome reveals microglial key events in amyotrophic lateral sclerosis. *Neurol Neuroimmunol Neuroinflamm* 7(5):e829
- Tasaki S, Xu J, Avey DR, Johnson L, Petyuk VA, Dawe RJ et al (2022) Inferring protein expression changes from mRNA in Alzheimer's dementia using deep neural networks. *Nat Commun* 13(1):655
- Johnson ECB, Carter EK, Dammer EB, Duong DM, Gerasimov ES, Liu Y et al (2022) Large-scale deep multi-layer analysis of Alzheimer's disease brain reveals strong proteomic disease-related changes not observed at the RNA level. *Nat Neurosci* 25(2):213–225
- Brooks BR, Miller RG, Swash M, Munsat TL (2000) Diseases WFO/NGoMN El escorial revisited: revised criteria for the diagnosis of amyotrophic lateral sclerosis. *Amyotroph Lateral Scler Other Motor Neuron Disord*. 1(5):293–299
- Niven E, Newton J, Foley J, Colville S, Swingler R, Chandran S et al (2015) Validation of the Edinburgh cognitive and behavioural amyotrophic lateral sclerosis screen (ECAS): a cognitive tool for motor disorders. *Amyotroph Lateral Scler Frontotemporal Degener* 16(3–4):172–179
- Black HA, Leighton DJ, Cleary EM, Rose E, Stephenson L, Colville S et al (2017) Genetic epidemiology of motor neuron disease-associated variants in the Scottish population. *Neurobiol Aging* 51:17.e811–178.e20

24. Tai HC, Serrano-Pozo A, Hashimoto T, Frosch MP, Spire-Jones TL, Hyman BT (2012) The synaptic accumulation of hyperphosphorylated tau oligomers in Alzheimer disease is associated with dysfunction of the ubiquitin-proteasome system. *Am J Pathol* 181(4):1426–1435
25. Hesse R, Hurtado ML, Jackson RJ, Eaton SL, Herrmann AG, Colom-Cadena M et al (2019) Comparative profiling of the synaptic proteome from Alzheimer's disease patients with focus on the APOE genotype. *Acta Neuropathol Commun* 7(1):214
26. Cox J, Mann M (2008) MaxQuant enables high peptide identification rates, individualized ppb-range mass accuracies and proteome-wide protein quantification. *Nat Biotechnol* 26(12):1367–1372
27. Cox J, Neuhauser N, Michalski A, Scheltema RA, Olsen JV, Mann M (2011) Andromeda: a peptide search engine integrated into the MaxQuant environment. *J Proteome Res* 10(4):1794–1805
28. Graham LC, Eaton SL, Brunton PJ, Atrih A, Smith C, Lamont DJ et al (2017) Proteomic profiling of neuronal mitochondria reveals modulators of synaptic architecture. *Mol Neurodegener* 12(1):77
29. Sherman BT, Hao M, Qiu J, Jiao X, Baseler MW, Lane HC et al (2022) DAVID: a web server for functional enrichment analysis and functional annotation of gene lists (2021 update). *Nucleic Acids Res*. <https://doi.org/10.1093/nar/gkac194>
30. Huang DW, Sherman BT, Lempicki RA (2009) Systematic and integrative analysis of large gene lists using DAVID bioinformatics resources. *Nat Protoc* 4(1):44–57
31. Kay KR, Smith C, Wright AK, Serrano-Pozo A, Pooler AM, Koffie R et al (2013) Studying synapses in human brain with array tomography and electron microscopy. *Nat Protoc* 8(7):1366–1380
32. Thevenaz P, Ruttimann UE, Unser M (1998) A pyramid approach to subpixel registration based on intensity. *IEEE Trans Image Process* 7(1):27–41
33. Piehowski PD, Petyuk VA, Orton DJ, Xie F, Moore RJ, Ramirez-Restrepo M et al (2013) Sources of technical variability in quantitative LC-MS proteomics: human brain tissue sample analysis. *J Proteome Res* 12(5):2128–2137
34. Aghamaleky Sarvestany A, Hunter G, Tavendale A, Lamont DJ, Llavero Hurtado M, Graham LC et al (2014) Label-free quantitative proteomic profiling identifies disruption of ubiquitin homeostasis as a key driver of Schwann cell defects in spinal muscular atrophy. *J Proteome Res* 13(11):4546–4557
35. Gillingwater TH, Ingham CA, Parry KE, Wright AK, Haley JE, Wishart TM et al (2006) Delayed synaptic degeneration in the CNS of Wlds mice after cortical lesion. *Brain* 129(Pt 6):1546–1556
36. Mutsaers CA, Lamont DJ, Hunter G, Wishart TM, Gillingwater TH (2013) Label-free proteomics identifies Calreticulin and GRP75/Mortalin as peripherally accessible protein biomarkers for spinal muscular atrophy. *Genome Med* 5(10):95
37. Roche SL, Sherman DL, Dissanayake K, Soucy G, Desmazieres A, Lamont DJ et al (2014) Loss of glial neurofascin 155 delays developmental synapse elimination at the neuromuscular junction. *J Neurosci* 34(38):12904–12918
38. Carlyle BC, Kandigian SE, Kreuzer J, Das S, Trombetta BA, Kuo Y et al (2021) Synaptic proteins associated with cognitive performance and neuropathology in older humans revealed by multiplexed fractionated proteomics. *Neurobiol Aging* 105:99–114
39. Bai B, Wang X, Li Y, Chen PC, Yu K, Dey KK et al (2020) Deep multilayer brain proteomics identifies molecular networks in Alzheimer's disease progression. *Neuron* 105(6):975–91.e7
40. Sorokina O, Mclean C, Croning MDR, Heil KF, Wysocka E, He X et al (2021) A unified resource and configurable model of the synapse proteome and its role in disease. *Sci Rep* 11(1):9967
41. Koopmans F, van Nierop P, Andres-Alonso M, Byrnes A, Cijssouw T, Coba MP et al (2019) SynGO: an evidence-based, expert-curated knowledge base for the synapse. *Neuron* 103(2):217–34.e4
42. Pirooznia M, Wang T, Avramopoulos D, Valle D, Thomas G, Huginir RL et al (2012) SynaptomeDB: an ontology-based knowledgebase for synaptic genes. *Bioinformatics* 28(6):897–899
43. Ge SX, Jung D, Yao R (2020) ShinyGO: a graphical gene-set enrichment tool for animals and plants. *Bioinformatics* 36(8):2628–2629
44. Raudvere U, Kolberg L, Kuzmin I, Arak T, Adler P, Peterson H et al (2019) g:Profiler: a web server for functional enrichment analysis and conversions of gene lists (2019 update). *Nucleic Acids Res* 47(W1):W191–W198
45. van Rheenen W, van der Spek RAA, Bakker MK, van Vugt JJFA, Hop PJ, Zwamborn RAJ et al (2021) Common and rare variant association analyses in amyotrophic lateral sclerosis identify 15 risk loci with distinct genetic architectures and neuron-specific biology. *Nat Genet* 53(12):1636–1648
46. Nguyen HP, Van Broeckhoven C, van der Zee J (2018) ALS genes in the genomic era and their implications for FTD. *Trends Genet* 34(6):404–423
47. Chia R, Chiò A, Traynor BJ (2018) Novel genes associated with amyotrophic lateral sclerosis: diagnostic and clinical implications. *Lancet Neurol* 17(1):94–102
48. Frick P, Sellier C, Mackenzie IRA, Cheng CY, Tahraoui-Bories J, Martinat C et al (2018) Novel antibodies reveal presynaptic localization of C9orf72 protein and reduced protein levels in C9orf72 mutation carriers. *Acta Neuropathol Commun* 6(1):72
49. Climer LK, Hendrix RD, Lupashin VV (2018) Conserved oligomeric golgi and neuronal vesicular trafficking. *Handb Exp Pharmacol* 245:227–247
50. Haase G, Rabouille C (2015) Golgi fragmentation in ALS Motor neurons new mechanisms targeting microtubules tethers and transport vesicles. *Front Neurosci* 9:448
51. Elamin M, Phukan J, Bede P, Jordan N, Byrne S, Pender N et al (2011) Executive dysfunction is a negative prognostic indicator in patients with ALS without dementia. *Neurology* 76(14):1263–1269
52. Yap K, Drakew A, Smilovic D, Rietsche M, Paul MH, Vuksic M et al (2020) The actin-modulating protein synaptotagmin mediates long-term survival of dendritic spines. *Elife*. <https://doi.org/10.7554/eLife.62944>
53. McCauley ME, Baloh RH (2019) Inflammation in ALS/FTD pathogenesis. *Acta Neuropathol* 137(5):715–730
54. Carroll MC (2004) The complement system in regulation of adaptive immunity. *Nat Immunol* 5(10):981–986
55. Presumey J, Bialas AR, Carroll MC (2017) Complement system in neural synapse elimination in development and disease. *Adv Immunol* 135:53–79
56. Hong S, Beja-Glasser VF, Nfonoyim BM, Frouin A, Li S, Ramakrishnan S et al (2016) Complement and microglia mediate early synapse loss in Alzheimer mouse models. *Science* 352(6286):712–716
57. Lin Z, Kim E, Ahmed M, Han G, Simmons C, Redhead Y et al (2021) MRI-guided histology of TDP-43 knock-in mice implicates parvalbumin interneuron loss, impaired neurogenesis and aberrant neurodevelopment in amyotrophic lateral sclerosis-frontotemporal dementia. *Brain Commun* 3(2):fcb114
58. Allodi I, Montañana-Rosell R, Selvan R, Löw P, Kiehn O (2021) Locomotor deficits in a mouse model of ALS are paralleled by loss of V1-interneuron connections onto fast motor neurons. *Nat Commun* 12(1):3251
59. Maekawa S, Al-Sarraj S, Kibble M, Landau S, Parnavelas J, Cotter D et al (2004) Cortical selective vulnerability in motor neuron disease: a morphometric study. *Brain* 127(Pt 6):1237–1251
60. Coyne AN, Zaeffel BL, Zarnescu DC (2017) Failure to deliver and translate—new insights into RNA dysregulation in ALS. *Front Cell Neurosci* 11:243
61. Liu-Yesucevitz L, Bassell GJ, Gitler AD, Hart AC, Klann E, Richter JD et al (2011) Local RNA translation at the synapse and in disease. *J Neurosci* 31(45):16086–16093
62. Glanzer J, Miyashiro KY, Sul JY, Barrett L, Belt B, Haydon P et al (2005) RNA splicing capability of live neuronal dendrites. *Proc Natl Acad Sci USA* 102(46):16859–16864
63. Ma XR, Prudencio M, Koike Y, Vatsavayai SC, Kim G, Harbinski F et al (2022) TDP-43 represses cryptic exon inclusion in the FTD-ALS gene UNC13A. *Nature* 603(7899):124–130
64. Brown AL, Wilkins OG, Keuss MJ, Hill SE, Zanovello M, Lee WC et al (2022) TDP-43 loss and ALS-risk SNPs drive mis-splicing and depletion of UNC13A. *Nature* 603(7899):131–137
65. Kaila K, Price TJ, Payne JA, Puskarjov M, Voipio J (2014) Cation-chloride cotransporters in neuronal development, plasticity and disease. *Nat Rev Neurosci* 15(10):637–654
66. Zucchi E, Bonetto V, Sorarù G, Martinelli I, Parchi P, Liguori R et al (2020) Neurofilaments in motor neuron disorders: towards promising diagnostic and prognostic biomarkers. *Mol Neurodegener* 15(1):58
67. Dukkupati SS, Garrett TL, Elbasiouny SM (2018) The vulnerability of spinal motoneurons and soma size plasticity in a mouse model of amyotrophic lateral sclerosis. *J Physiol* 596(9):1723–1745

68. Kano SI, Choi EY, Dohi E, Agarwal S, Chang DJ, Wilson AM et al (2019) Glutathione S-transferases promote proinflammatory astrocyte-microglia communication during brain inflammation. *Sci Signal*. <https://doi.org/10.1126/scisignal.aar2124>
69. Broadhead MJ, Bonthron C, Waddington J, Smith WV, Lopez MF, Burley S et al (2021) Selective vulnerability of tripartite synapses in amyotrophic lateral sclerosis. *Acta Neuropathol* 212(1):8
70. Liang F, Liang J, Wang WQ, Sun JP, Udho E, Zhang ZY (2007) PRL3 promotes cell invasion and proliferation by down-regulation of Csk leading to Src activation. *J Biol Chem* 282(8):5413–5419
71. Urwyler O, Izadifar A, Vandenberghe S, Sachse S, Misbaer A, Schmucker D (2019) Branch-restricted localization of phosphatase Prl-1 specifies axonal synaptogenesis domains. *Science*. <https://doi.org/10.1126/science.aau9952>
72. Wang T, Hong W (2002) Interorganellar regulation of lysosome positioning by the Golgi apparatus through Rab34 interaction with Rab-interacting lysosomal protein. *Mol Biol Cell* 13(12):4317–4332
73. Goldenberg NM, Silverman M (2009) Rab34 and its effector munc13-2 constitute a new pathway modulating protein secretion in the cellular response to hyperglycemia. *Am J Physiol Cell Physiol* 297(4):C1053–C1058
74. Kaspapour B, Gronow A, Bleck CK, Hong W, Gutierrez MG (2012) Size-dependent mechanism of cargo sorting during lysosome-phagosome fusion is controlled by Rab34. *Proc Natl Acad Sci U S A* 109(50):20485–20490
75. Varoqueaux F, Sigler A, Rhee JS, Brose N, Enk C, Reim K et al (2002) Total arrest of spontaneous and evoked synaptic transmission but normal synaptogenesis in the absence of Munc13-mediated vesicle priming. *Proc Natl Acad Sci U S A* 99(13):9037–9042
76. Ji YX, Huang Z, Yang X, Wang X, Zhao LP, Wang PX et al (2018) The deubiquitinating enzyme cylindromatosis mitigates nonalcoholic steatohepatitis. *Nat Med* 24(2):213–223
77. Dobson-Stone C, Hallupp M, Shahheydari H, Ragagnin AMG, Chatterton Z, Carew-Jones F et al (2020) CYLD is a causative gene for frontotemporal dementia - amyotrophic lateral sclerosis. *Brain* 143(3):783–799
78. Tábuas-Pereira M, Santana I, Kun-Rodrigues C, Bras J, Guerreiro R (2020) CYLD variants in frontotemporal dementia associated with severe memory impairment in a Portuguese cohort. *Brain* 143(8):e67
79. Gu X, Chen Y, Wei Q, Hou Y, Cao B, Zhang L et al (2021) Rare CYLD variants in chinese patients with amyotrophic lateral sclerosis. *Front Genet* 12:740052
80. Oyston LJ, Chatterton Z, Hallupp M, Rajan N, Kwok JB, Dobson-Stone C (2020) Reply: CYLD variants in frontotemporal dementia associated with severe memory impairment in a Portuguese cohort. *Brain* 143(8):e68
81. Hao MQ, Xie LJ, Leng W, Xue RW (2019) Trim47 is a critical regulator of cerebral ischemia-reperfusion injury through regulating apoptosis and inflammation. *Biochem Biophys Res Commun* 515(4):651–657
82. Putkey JA, Waxham MN, Gaertner TR, Brewer KJ, Goldsmith M, Kubota Y et al (2008) Acidic/IQ motif regulator of calmodulin. *J Biol Chem* 283(3):1401–1410
83. Utal AK, Stopka AL, Roy M, Coleman PD (1998) PEP-19 immunohistochemistry defines the basal ganglia and associated structures in the adult human brain, and is dramatically reduced in Huntington's disease. *Neuroscience* 86(4):1055–1063
84. Wei P, Blundon JA, Rong Y, Zakharenko SS, Morgan JI (2011) Impaired locomotor learning and altered cerebellar synaptic plasticity in pep-19/PCP4-null mice. *Mol Cell Biol* 31(14):2838–2844
85. Rosa JM, Farré-Alins V, Ortega MC, Navarrete M, Lopez-Rodriguez AB, Palomino-Antolin A et al (2021) TLR4 pathway impairs synaptic number and cerebrovascular functions through astrocyte activation following traumatic brain injury. *Br J Pharmacol* 178(17):3395–3413
86. Lee JY, Lee JD, Phipps S, Noakes PG, Woodruff TM (2015) Absence of toll-like receptor 4 (TLR4) extends survival in the hSOD1 G93A mouse model of amyotrophic lateral sclerosis. *J Neuroinflammation* 12:90
87. Ribeiro P, Castro MV, Perez M, Cartarozzi LP, Spejo AB, Chiarotto GB et al (2020) Toll-like receptor 4 (TLR4) influences the glial reaction in the spinal cord and the neural response to injury following peripheral nerve crush. *Brain Res Bull* 155:67–80
88. DaRosa PA, Wang Z, Jiang X, Pruneda JN, Cong F, Kleivt RE et al (2015) Allosteric activation of the RNF146 ubiquitin ligase by a poly(ADP-ribosylation) signal. *Nature* 517(7533):223–226
89. Kim DS, Camacho CV, Kraus WL (2021) Alternate therapeutic pathways for PARP inhibitors and potential mechanisms of resistance. *Exp Mol Med* 53(1):42–51
90. David KK, Andrabi SA, Dawson TM, Dawson VL (2009) Parthanatos, a messenger of death. *Front Biosci (Landmark Ed)* 14(3):1116–1128
91. McGurk L, Mojsilovic-Petrovic J, Van Deerlin VM, Shorter J, Kalb RG, Lee VM et al (2018) Nuclear poly(ADP-ribose) activity is a therapeutic target in amyotrophic lateral sclerosis. *Acta Neuropathol Commun* 6(1):84
92. McGurk L, Rifai OM, Bonini NM (2019) Poly(ADP-Ribosylation) in age-related neurological disease. *Trends Genet* 35(8):601–613
93. Andrabi SA, Kang HC, Haince JF, Lee YI, Zhang J, Chi Z et al (2011) Ilduna protects the brain from glutamate excitotoxicity and stroke by interfering with poly(ADP-ribose) polymer-induced cell death. *Nat Med* 17(6):692–699
94. Lee HW, Choi J, Shin H, Kim K, Yang J, Na M et al (2008) Preso, a novel PSD-95-interacting FERM and PDZ domain protein that regulates dendritic spine morphogenesis. *J Neurosci* 28(53):14546–14556
95. Hu JH, Yang L, Kammermeier PJ, Moore CG, Brakeman PR, Tu J et al (2012) Preso1 dynamically regulates group I metabotropic glutamate receptors. *Nat Neurosci* 15(6):836–844
96. Piard J, Hu JH, Campeau PM, Rzonca S, Van Esch H, Vincent E et al (2018) FRMPD4 mutations cause X-linked intellectual disability and disrupt dendritic spine morphogenesis. *Hum Mol Genet* 27(4):589–600
97. Andrés-Benito P, Gelpi E, Povedano M, Santpere G, Ferrer I (2018) Gene expression profile in frontal cortex in sporadic frontotemporal lobar degeneration-TDP. *J Neuropathol Exp Neurol* 77(7):608–627
98. Lee JD, McDonald TS, Fung JNT, Woodruff TM (2020) Absence of receptor for advanced glycation end product (RAGE) reduces inflammation and extends survival in the hSOD1 G93A mouse model of amyotrophic lateral sclerosis. *Mol Neurobiol* 57(10):4143–4155
99. MacLean M, Juranek J, Cuddapah S, López-Diez R, Ruiz HH, Hu J et al (2021) Microglia RAGE exacerbates the progression of neurodegeneration within the SOD1 G93A murine model of amyotrophic lateral sclerosis in a sex-dependent manner. *J Neuroinflamm* 18(1):139
100. Turner MR, Rabiner EA, Hammers A, Al-Chalabi A, Grasby PM, Shaw CE et al (2005) [¹¹C]-WAY100635 PET demonstrates marked 5-HT_{1A} receptor changes in sporadic ALS. *Brain* 128(Pt 4):896–905
101. Balendra R, Isaacs AM (2018) C9orf72-mediated ALS and FTD: multiple pathways to disease. *Nat Rev Neurol* 14(9):544–558
102. Butti Z, Pan YE, Giacomotto J, Patten SA (2021) Reduced C9orf72 function leads to defective synaptic vesicle release and neuromuscular dysfunction in zebrafish. *Commun Biol* 4(1):792
103. Jensen BK, Schuldi MH, McAvooy K, Russell KA, Boehringer A, Curran BM et al (2020) Synaptic dysfunction induced by glycine-alanine dipeptides in C9orf72-ALS/FTD is rescued by SV2 replenishment. *EMBO Mol Med* 12(5):e10722
104. Perkins EM, Burr K, Banerjee P, Mehta AR, Dando O, Selvaraj BT et al (2021) Altered network properties in C9ORF72 repeat expansion cortical neurons are due to synaptic dysfunction. *Mol Neurodegener* 16(1):13
105. Catanese A, Rajkumar S, Sommer D, Freisem D, Wirth A, Aly A et al (2021) Synaptic disruption and CREB-regulated transcription are restored by K. *EMBO Mol Med* 13(7):e13131
106. Starr A, Sattler R (2018) Synaptic dysfunction and altered excitability in C9ORF72 ALS/FTD. *Brain Res* 1693(Pt A):98–108
107. Nizzardo M, Taiana M, Rizzo F, Aguilu Benitez J, Nijssen J, Allodi I et al (2020) Synaptotagmin 13 is neuroprotective across motor neuron diseases. *Acta Neuropathol* 139(5):837–853
108. Fricker LD, McKinzie AA, Sun J, Curran E, Qian Y, Yan L et al (2000) Identification and characterization of proSAAS, a granin-like neuroendocrine peptide precursor that inhibits prohormone processing. *J Neurosci* 20(2):639–648
109. Kikuchi K, Arawaka S, Koyama S, Kimura H, Ren CH, Wada M et al (2003) An N-terminal fragment of ProSAAS (a granin-like neuroendocrine peptide precursor) is associated with tau inclusions in Pick's disease. *Biochem Biophys Res Commun* 308(3):646–654
110. Wada M, Ren CH, Koyama S, Arawaka S, Kawakatsu S, Kimura H et al (2004) A human granin-like neuroendocrine peptide precursor

- (proSAAS) immunoreactivity in tau inclusions of Alzheimer's disease and parkinsonism-dementia complex on Guam. *Neurosci Lett* 356(1):49–52
111. Jahn H, Wittke S, Zürlbig P, Raedler TJ, Arlt S, Kellmann M et al (2011) Peptide fingerprinting of Alzheimer's disease in cerebrospinal fluid: identification and prospective evaluation of new synaptic biomarkers. *PLoS One* 6(10):e26540
 112. Davidsson P, Sjögren M, Andreasen N, Lindbjer M, Nilsson CL, Westman-Brinkmalm A et al (2002) Studies of the pathophysiological mechanisms in frontotemporal dementia by proteome analysis of CSF proteins. *Brain Res Mol Brain Res* 109(1–2):128–133
 113. Hoshino A, Helwig M, Rezaei S, Berridge C, Eriksen JL, Lindberg I (2014) A novel function for proSAAS as an amyloid anti-aggregant in Alzheimer's disease. *J Neurochem* 128(3):419–430
 114. Jarvela TS, Lam HA, Helwig M, Lorenzen N, Otzen DE, McLean PJ et al (2016) The neural chaperone proSAAS blocks α -synuclein fibrillation and neurotoxicity. *Proc Natl Acad Sci U S A* 113(32):E4708–E4715
 115. Mollieux A, Temirov J, Lee J, Coughlin M, Kanagaraj AP, Kim HJ et al (2015) Phase separation by low complexity domains promotes stress granule assembly and drives pathological fibrillization. *Cell* 163(1):123–133
 116. Freibaum BD, Taylor JP (2017) The role of dipeptide repeats in C9ORF72-related ALS-FTD. *Front Mol Neurosci* 10:35
 117. Brady OA, Zheng Y, Murphy K, Huang M, Hu F (2013) The frontotemporal lobar degeneration risk factor, TMEM106B, regulates lysosomal morphology and function. *Hum Mol Genet* 22(4):685–695
 118. Van Deerlin VM, Sleiman PM, Martinez-Lage M, Chen-Plotkin A, Wang LS, Graff-Radford NR et al (2010) Common variants at 7p21 are associated with frontotemporal lobar degeneration with TDP-43 inclusions. *Nat Genet* 42(3):234–239
 119. Gallagher MD, Suh E, Grossman M, Elman L, McCluskey L, Van Swieten JC et al (2014) TMEM106B is a genetic modifier of frontotemporal lobar degeneration with C9orf72 hexanucleotide repeat expansions. *Acta Neuropathol* 127(3):407–418
 120. Klein ZA, Takahashi H, Ma M, Stagi M, Zhou M, Lam TT et al (2017) Loss of TMEM106B ameliorates lysosomal and frontotemporal dementia-related phenotypes in progranulin-deficient mice. *Neuron* 95(2):281–96.e6
 121. Jiang YX, Cao Q, Sawaya MR, Abskharon R, Ge P, DeTure M et al (2022) Amyloid fibrils in disease FTLTDP are composed of TMEM106B not TDP-43. *Nature*. <https://doi.org/10.1038/s41586-022-04670-9>
 122. Schwenk BM, Lang CM, Höggl S, Tahirovic S, Orozco D, Rentzsch K et al (2014) The FTLTDP risk factor TMEM106B and MAP6 control dendritic trafficking of lysosomes. *EMBO J* 33(5):450–467

Publisher's Note

Springer Nature remains neutral with regard to jurisdictional claims in published maps and institutional affiliations.

Ready to submit your research? Choose BMC and benefit from:

- fast, convenient online submission
- thorough peer review by experienced researchers in your field
- rapid publication on acceptance
- support for research data, including large and complex data types
- gold Open Access which fosters wider collaboration and increased citations
- maximum visibility for your research: over 100M website views per year

At BMC, research is always in progress.

Learn more biomedcentral.com/submissions

